University of Zagreb

Faculty of Mechanical Engineering and Naval Architecture

GRADUATE WORK

Mentor

Zdravko Virag

Daniel Filkovic

Zagreb. 2008

Summary

In this graduate work a panel method variant has been developed for calculating potential flow of three-dimensional aerodynamic configurations. The core of the program is discretisation of the geometry with combination of quadrilateral panels with constant source and constant dipole and finding their values with the appropriate boundary condition. From the dipole values it is then easy to calculate velocity and pressure and at the end, aerodynamic coefficients which are the final goal.

The program is tested on wing and aircraft configuration, where obtained results are compared with commercial package FLUENT with satisfactory deviations.

Keywords: potential flow, panel method, aircraft configuration, FLUENT, finite volume method

Contents

1. INTRODUCTION 1

2. THEORETICAL BASIS 2

2.1. The main equations of fluid dynamics 2
2.2. Navier-Stokes equations 2
2.3. The equations that describe the potential flow 3
2.4. Fundamentals of inviscid, incompressible flow 5

3. EQUATIONS (PARTS) OF THE PROGRAM 6

3.1. Calculating geometry characteristics of the mesh 6
3.2. Influence coefficients calculation 10
3.3. Solution of system of equations 15
3.4. Calculation of velocity, pressure and forces 16

4. OVERVIEW OF 3D PANEL METHOD RESULTS 18

4.1. Analysis of convergence of solutions with respect to mesh density 18
4.1.1. Convergence vs. number of panels per wingspan 19
4.1.2. Convergence vs. number of panels per wing airfoil 21
4.2. Results of 3D panel method and FLUENT for aircraft configuration. 25
4.2.1. Description of selected configuration 25
4.2.2. Geometry discretization for panel method 27
4.2.3. Convergence of solution with respect to "far field" coefficient 28
4.2.4. Discretizing aircraft geometry for FLUENT 30
4.2.5. Convergence testing in FLUENT 32
4.2.6. Comparison of results 34

CONCLUSION 60

List of Figures

Figure 2-1 *Transformation from aircraft to aerodynamic coordinate system* ... *4*
Figure 2-2 *Division of flow to viscous and inviscid region* ... *5*
Figure 3-1 *The chosen coordinate system* ... *6*
Figure 3-2 *Panel indexing* ... *7*
Figure 3-3 *Collocation point and unit vectors of panel* ... *8*
Figure 3-4 *Quadrilateral panel* ... *11*
Figure 3-5 *Kutta condition on trailing edge of the wing* ... *14*
Figure 4-1 *Geometry of the analyzed wing* ... *18*
Figure 4-2 *a) coarse, b) optimal and c) fine wing mesh* ... *23*
Figure 4-3 *Three projections of selected aircraft configuration* ... *26*
Figure 4-4 *Three meshes: a) coarse b) optimal and c) fine* ... *27*
Figure 4-5 *Flow domain in FLUENT* ... *30*
Figure 4-6 *Different mesh densities for FLUENT analysis* ... *31*
Figure 4-7 *Selected FLUENT mesh* ... *33*
Figure 4-8 *Pressure coefficient distribution for a) FLUENT b) 3D Panel Method* ... *59*

List of diagrams

Diagram 4-1 *Longitudinal force coefficient vs. half wing panel number* ... 19
Diagram 4-2 *Vertical force coefficient vs. half wing panel number* ... 20
Diagram 4-3 *Pitching moment coefficient vs. half wing panel number* ... 20
Diagram 4-4 *Longitudinal force coefficient vs. airfoil panel number* ... 21
Diagram 4-5 *Vertical force coefficient vs. airfoil panel number* ... 22
Diagram 4-6 *Pitching moment coefficient vs. airfoil panel number* ... 22
Diagram 4-7 *Pressure coefficient for coarse (blue), optimal (black) and fine (red) wing* ... 24
Diagram 4-8 *Computation time vs. mesh density* ... 24
Diagram 4-9 *Longitudinal force coefficient vs. "far field" coefficient* ... 28
Diagram 4-10 *Vertical force coefficient vs. "far field" coefficient* ... 28
Diagram 4-11 *Pitching moment coefficient vs. "far field" coefficient* ... 29
Diagram 4-12 *Influence coefficients calculation time vs. "far field" coefficient* ... 29
Diagram 4-13 *Computation time in FLUENT vs. number of elements* ... 32
Diagram 4-14 *Convergence results in FLUENT* ... 33
Diagram 4-15 *Lift coefficient vs. angle of attack* ... 36
Diagram 4-16 *Drag coefficient vs. angle of attack* ... 36
Diagram 4-17 *Pitching moment coefficient vs. angle of attack* ... 37
Diagram 4-18 *Lateral force coefficient vs. sideslip angle* ... 37
Diagram 4-19 *Rolling moment coefficient vs. sideslip angle* ... 38
Diagram 4-20 *Yaw moment coefficient vs. sideslip angle* ... 38
Diagram 4-21 *Drag coefficient vs. angle of attack for wing* ... 44
Diagram 4-22 *Drag coefficient vs. angle of attack for horizontal stabilizer* ... 44
Diagram 4-23 *Drag coefficient vs. angle of attack for fuselage* ... 45
Diagram 4-24 *Drag coefficient vs. angle of attack for vertical stabilizer* ... 45
Diagram 4-25 *Lift coefficient vs. attack of angle for wing* ... 46
Diagram 4-26 *Lift coefficient vs. angle of attack for horizontal stabilizer* ... 46
Diagram 4-27 *Lift coefficient vs. angle of attack for fuselage* ... 47
Diagram 4-28 *Lift coefficient vs. angle of attack for vertical stabilizer* ... 47
Diagram 4-29 *Pitching moment coefficient vs. angle of attack for wing* ... 48
Diagram 4-30 *Pitching moment coefficient vs. angle of attack for horizontal stabilizer* ... 48
Diagram 4-31 *Pitching moment coefficient vs. angle of attack for fuselage* ... 49
Diagram 4-32 *Pitching moment coefficient vs. angle of attack for vertical stabilizer* ... 49
Diagram 4-33 *Rolling moment coefficient vs. sideslip angle for right wing* ... 50
Diagram 4-34 *Rolling moment coefficient vs. sideslip angle for left wing* ... 50
Diagram 4-35 *Rolling moment coefficient vs. sideslip angle for right horizontal stabilizer* ... 51
Diagram 4-36 *Rolling moment coefficient vs. sideslip angle for left horizontal stabilizer* ... 51
Diagram 4-37 *Rolling moment coefficient vs. sideslip angle for fuselage* ... 52
Diagram 4-38 *Rolling moment coefficient vs. sideslip angle for vertical stabilizer* ... 52

Diagram 4-39 Yaw moment coefficient vs. sideslip angle for right wing 53
Diagram 4-40 Yaw moment coefficient vs. sideslip angle for left wing 53
Diagram 4-41 Yaw moment coefficient vs. sideslip angle for right horizontal stabilizer 54
Diagram 4-42 Yaw moment coefficient vs. sideslip angle for left horizontal stabilizer 54
Diagram 4-43 Yaw moment coefficient vs. sideslip angle for fuselage 55
Diagram 4-44 Yaw moment coefficient vs. sideslip angle for vertical stabilizer 55
Diagram 4-45 Lateral force coefficient vs. sideslip angle for right wing 56
Diagram 4-46 Lateral force coefficient vs. sideslip angle for left wing 56
Diagram 4-47 Lateral force coefficient vs. sideslip angle for right horizontal stabilizer 57
Diagram 4-48 Lateral force coefficient vs. sideslip angle for left horizontal stabilizer 57
Diagram 4-49 Lateral force coefficient vs. sideslip angle for fuselage 58
Diagram 4-50 Lateral force coefficient vs. sideslip angle for vertical stabilizer 58

List of Tables

Table 4-1 *Geometric characteristics of selected aircraft configuration* *25*
Table 4-2 *Aerodynamic coefficients used for comparison* *34*
Table 4-3 *Aerodynamic coefficients in FLUENT and 3D panel method* *35*
Table 4-4 *Longitudinal analysis coefficients of aircraft components* *2*
Table 4-5 *Lateral analysis coefficients of aircraft components* *3*

Symbols

ρ	Fluid density
v_i	Velocity in i direction
x_i	i Coordinate
f_i	External mass force
σ_{ji}	Stress tensor
$\boldsymbol{\psi}$	Vector potential
φ	Scalar potential
p	Pressure
F_i	Force in i direction
M_i	Moment in i axis
$\mathbf{n}$	Normal unit vector
$\mathbf{u}$	Longitudinal unit vector
$\mathbf{p}$	Transverse unit vector
$\mathbf{o}$	Perpendicular unit vector
M	Number of longitudinal panels
N	Number of lateral panels
S_k	Surface of k panel
c_x, c_y, c_z	Collocation points coordinates
$\mathbf{x}_{i\,\mathrm{glob}}$	Coordinates of i corner of panel in global coordinate system
$\mathbf{x}_{i\,\mathrm{lok}}$	Coordinates of i corner of panel in local coordinate system
Φ	Panel induced potential
σ	Constant source strength
μ	Constant dipole strength
$\mathbf{V}_\infty$	Free stream velocity components
V_∞	Free stream velocity value
$\mathbf{c}_{\mathrm{RHS}}$	‘‘Right hand side" vector
$\mathbf{a}$	Dipole influence coefficients matrix
$\mathbf{b}$	Source influence coefficients matrix
q_u, q_p, q_o	induced velocities in the longitudinal, transverse and perpendicular direction

g_u, g_o	Free stream velocity components in longitudinal and perpendicular direction
c_p	Pressure coefficient
F_i	Forces on body in i direction (i = x, y, z)
O	Number of panels
q	Dynamic (reference) pressure
M_L	Roll moment (about longitudinal X axis)
M_M	Pitch moment (about lateral Y axis)
M_N	Yaw moment (about vertical Z axis)
C_i	Force coefficient on body in *i* direction (i = x, y, z)
C_L	Roll moment coefficient
C_M	Pitch moment coefficient
C_N	Yaw moment coefficient
C_L	Lift coefficient
C_D	Drag coefficient
S_{ref}	Wing area (reference)
b_{span}	Wing span (reference)
c_{SAT}	Mean aerodynamic chord (reference)
A	Aspect ratio

Declaration

I declare that this graduate work is my own and made by using knowledge gained during the study and the literature mentioned in the work with the expert help of a mentor prof. PhD. Zdravko Virag and dipl. ing. Severino Krizmanic. For this, I am sincerely grateful to them.

1. INTRODUCTION

A classic problem in aerodynamics is to determine the forces and moments on aircraft due to the airflow. The most accurate way is to test the very aircraft, but it involves building a prototype, and is the most expensive and (in design stage) unacceptable solution. Next is testing in the wind tunnel and that is the pinnacle of technology, but it is very expensive and, from the viewpoint of analysis and optimization, a very slow method.

The panel method is relatively old numerical method which draws its beginnings with first appearance of computers. The method solves potential flow about aircraft configuration which, if one extends the problem with boundary layer solution near the walls, enables to solve most problems in the linear behavior of the aircraft.

The last couple of decades, the panel method is suppressed and today, finite volume method (hereinafter FVM) is probably the most widely used method for numerical flow analysis. The method is based on Navier-Stokes equations discretization by finite volumes (cells). The advantages of FVM are ability to analyze all cases of aircraft flow at all speeds - viscous (turbulent) and compressible flow. Because FVM is using discretized space, as opposed to the panel method where the discretization occurs only on the surface of the body, FVM is much slower method, therefore making panel method still present.

In this work a panel method is being developed whose results will be compared to FVM with inviscid, incompressible flow model.

2. THEORETICAL BASIS

This chapter will present the main equations describing the flow in this paper. The equations will be written with index notation.

2.1. The main equations of fluid dynamics

The first main equation is the law of conservation of mass:

$$\frac{\partial \rho}{\partial t} + \frac{\partial (\rho v_i)}{\partial x_i} = 0 \tag{1.1}$$

Equation (1.1) for incompressible fluid takes a simpler form since incompressible fluid has constant density:

$$\frac{\partial v_i}{\partial x_i} = 0 \tag{1.2}$$

The second main equation is the low of conservation of momentum:

$$\frac{\partial (\rho v_i)}{\partial t} + \frac{\partial (\rho v_j v_i)}{\partial x_j} = \rho f_i + \frac{\partial \sigma_{ji}}{\partial x_j} \tag{1.3}$$

2.2. Navier-Stokes equations

Introducing Newton viscosity law and the continuity equation in the law of conservation of momentum we get the well-known Navier-Stokes equations for incompressible fluid:

$$\frac{\partial v_x}{\partial x} + \frac{\partial v_y}{\partial y} + \frac{\partial v_z}{\partial z} = 0$$

$$\begin{aligned}
\rho\left(\frac{\partial v_x}{\partial t} + v_x\frac{\partial v_x}{\partial x} + v_y\frac{\partial v_x}{\partial y} + v_z\frac{\partial v_x}{\partial z}\right) &= -\frac{\partial p}{\partial x} + \mu\left(\frac{\partial^2 v_x}{\partial x^2} + \frac{\partial^2 v_x}{\partial y^2} + \frac{\partial^2 v_x}{\partial z^2}\right) + \rho f_x \\
\rho\left(\frac{\partial v_y}{\partial t} + v_x\frac{\partial v_y}{\partial x} + v_y\frac{\partial v_y}{\partial y} + v_z\frac{\partial v_y}{\partial z}\right) &= -\frac{\partial p}{\partial x} + \mu\left(\frac{\partial^2 v_y}{\partial x^2} + \frac{\partial^2 v_y}{\partial y^2} + \frac{\partial^2 v_y}{\partial z^2}\right) + \rho f_y \\
\rho\left(\frac{\partial v_z}{\partial t} + v_x\frac{\partial v_z}{\partial x} + v_y\frac{\partial v_z}{\partial y} + v_z\frac{\partial v_z}{\partial z}\right) &= -\frac{\partial p}{\partial x} + \mu\left(\frac{\partial^2 v_z}{\partial x^2} + \frac{\partial^2 v_z}{\partial y^2} + \frac{\partial^2 v_z}{\partial z^2}\right) + \rho f_z
\end{aligned} \tag{1.4}$$

These equations are used in the FLUENT software package with, in our case, viscosity disregarded.

2.3. The equations that describe the potential flow

If we assume potential flow, equation 1.2 that represents continuity equation becomes

$$\frac{\partial^2 \varphi}{\partial x_i^2} = 0 \tag{1.5}$$

that is called the Laplace equation. Value φ in equation

$$v_i = \frac{\partial \varphi}{\partial x_i} \tag{1.6}$$

is called scalar speed potential. It can be easily proved that potential flow is irrotational.

Another important equation comes from the law of conservation of momentum for irrotational and inviscid flow (Euler equation) for the steady flow

$$\frac{v^2}{2} + \frac{p}{\rho} + gz = const \tag{1.7}$$

and is called the Euler-Bernoulli equation.

By solving equation (1.5) we get velocity field and by using equation (1.7) we get pressure field.

A very important property of the Laplace equation is that sum of any two solutions of that equation forms solution as well. This means that the flow can be arranged to present the sum of singularities whose values are found by satisfying appropriate boundary condition. This is important because the method presented in this work consists precisely of the combination of quadrilateral panel sources and dipoles distributed over the surface of the aerodynamic body.

Integrating the pressure over the surface of the body we get total forces and moments acting on the body:

$$F_i = -\int_S p n_i dS \tag{1.8}$$

$$M_i = -\int_S \varepsilon_{ijk} x_j n_k p dS \tag{1.9}$$

where p is the pressure, n_k normal unit vector component in k direction, and x_j distance from the reference point.

Force and moment coefficients are calculated according to the following terms:

$$C_X = \frac{F_X}{qS_{\text{ref}}},\ C_Y = \frac{F_Y}{qS_{\text{ref}}},\ C_Z = \frac{F_Z}{qS_{\text{ref}}}$$

$$C_l = \frac{M_l}{qS_{\text{ref}}b_{\text{span}}},\ C_m = \frac{M_m}{qS_{\text{ref}}c_{\text{SAT}}},\ C_n = \frac{M_n}{qS_{\text{ref}}b_{\text{span}}} \tag{1.10}$$

where S_{ref} is the reference area (wing), c_{SAT} reference length (the mean aerodynamic chord), b_{span} the reference length (wing span) and q reference pressure (dynamic).

The forces of lift and drag are defined in the aerodynamic coordinate system ($Ox_Ay_Az_A$) by rotating coordinate system of the aircraft ($Oxyz$), first by angle of attack (α) around *y* axis and then by side-slip angle (β) around z_A axis (Figure 2-1).

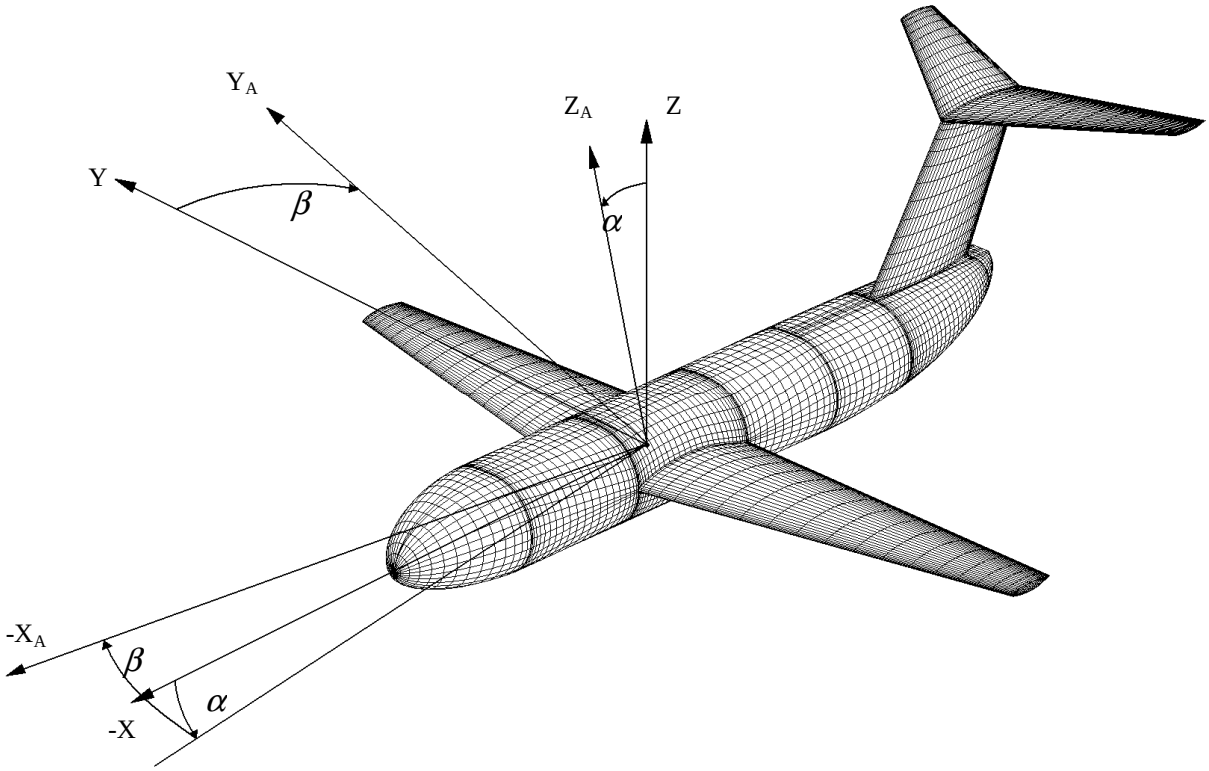

Figure 2-1 Transformation from aircraft to aerodynamic coordinate system

Since lift and drag forces in this paper are monitored only in longitudinal analysis where only angle of attack is changing, transformation is:

$$\begin{bmatrix} C_L \\ C_D \end{bmatrix} = \begin{bmatrix} \cos\alpha & -\sin\alpha \\ \sin\alpha & \cos\alpha \end{bmatrix} \begin{bmatrix} C_Z \\ C_X \end{bmatrix} \tag{1.11}$$

2.4. Fundamentals of inviscid, incompressible flow

Each velocity field can be represented by scalar and vector potential in the form of:

$$v_i = \frac{\partial \varphi}{\partial x_i} + \varepsilon_{ijk} \frac{\partial \psi_k}{\partial x_j} \tag{1.12}$$

where first part of right side represents solution to potential flow which is irrotational, and second part is sourceless and represents vorticity, but does not disrupt the continuity equation.

This is very important since this way circulation around the airfoil is introduced allowing calculation of lift.

In the case of three-dimensional body this circulation would represent a vortex line across wing span. Very important theorem, called the second Helmholtz theorem, says that the vortex tube cannot have a beginning or ending within the fluid. Bearing this in mind, the vortex line across wing span must turn down stream at wing tips. This phenomenon is physically visible in the form of vortices at the edges of aircraft wings.

It is important to note that the viscosity can be neglected in the area near the body wall (boundary layer), but since its thickness is relatively small, it will not significantly affect external potential flow (Figure 2.2).

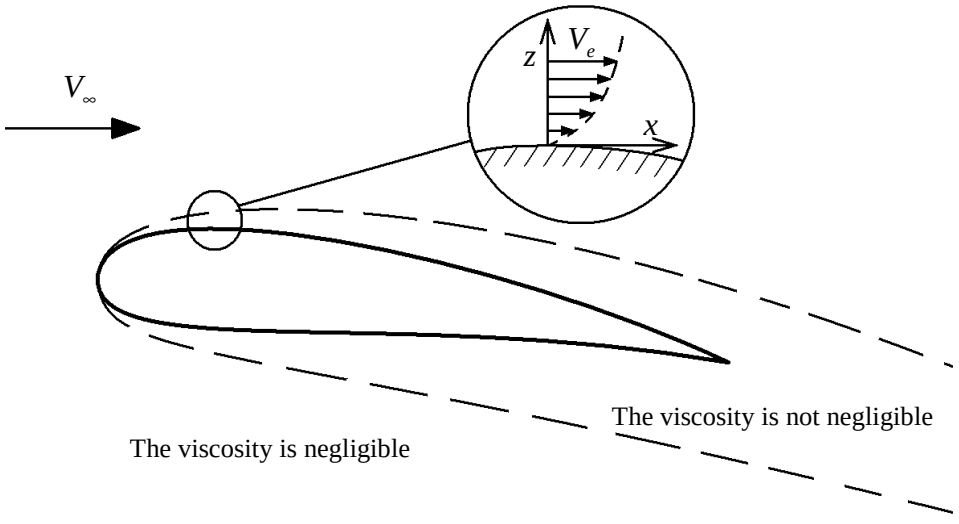

Figure 2-2 Division of flow to viscous and inviscid region

3. EQUATIONS (PARTS) OF THE PROGRAM

3D panel method program is written in a programming language MATLAB. Matlab is a very useful engineering tool with programming language like "C" and FORTRAN with a good post-processing capabilities or presentation of results.

Since the preparation of the mesh or geometry discretizing (pre-processing) is a very complicated task that involves, at least ready geometry made externally, and then its discretization, for this work "handmade" mesh is prepared which will be presented in Chapter 4.

3.1. Calculating geometry characteristics of the mesh

First of all, it is important to define global coordinate system that will be used in the program. This is right Cartesian coordinate system with x-axis pointing from nose to tail, y-axis direction in right wing span direction and z-axis pointing vertically as can be seen on aircraft configuration shown in Figure 3-1.

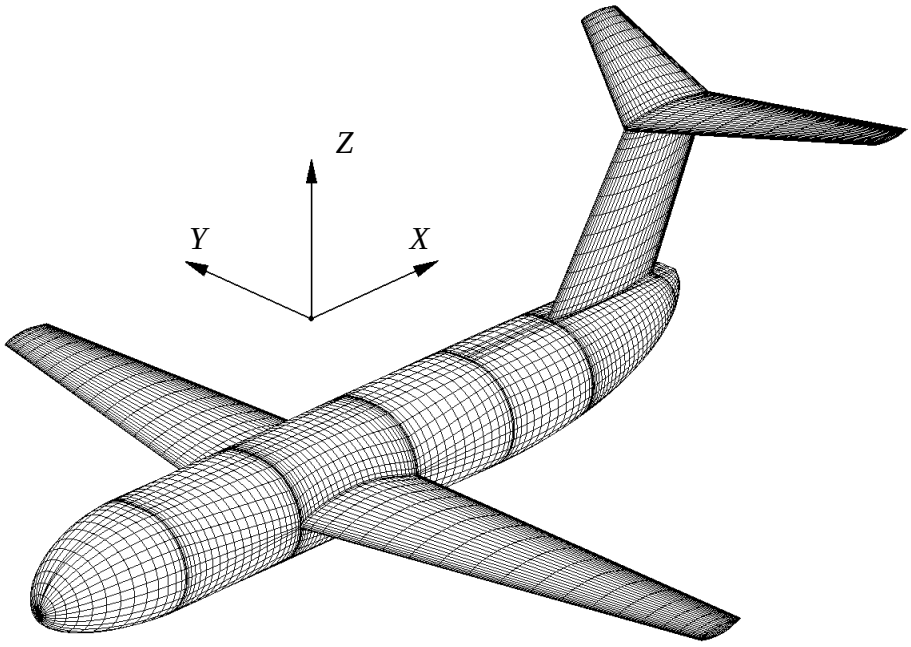

Figure 3-1 The chosen coordinate system

Geometry is discretized as structured mesh, with two counters; "i" – counter of number of panels per chord and "j" – counter of number of panels per span that defines the position of the panel. Labeling of the panel is very important and must be adopted by convention.

In Figure 3-2 wing is showed with convention of indexing panels. Indexing panel vertices is equivalent to indexing the panel with one difference, the number of vertices is by 1 higher than number of panels.

Bearing that in mind, mesh will mathematically consist of a matrix if geometric component can be unfolded into rectangular patch with form $M \times N$. If mesh cannot be unfolded into rectangular patch, as is case for this aircraft configuration mesh geometry is formed by "array" matrix of third order $M \times N \times komp$ where M and N are maximum number of transverse and longitudinal panels and $komp$ the number of components that will form the geometry. Again, if it comes to the vertices of the panel coordinates, the matrix takes the form of third order $(M+1)\times(N+1)\times komp$ for each of the three spatial coordinates x, y, z.

The calculation of panel surface is done by module of cross product of panel diagonals with following expression:

$$S = \frac{|\mathbf{A}\times\mathbf{B}|}{2} \tag{3.1}$$

where S is surface, and $\mathbf{A}$ and $\mathbf{B}$ panel diagonals.

If influenced point is located at distance from panel greater then $FF \cdot D$, where FF is "far field" coefficient and D length of larger panel diagonal, then the panel is substituted by point singularity. This is used for reducing calculation time and here the value of $FF = 5$ is chosen, which has proven enough in chapter 4. and also in [1].

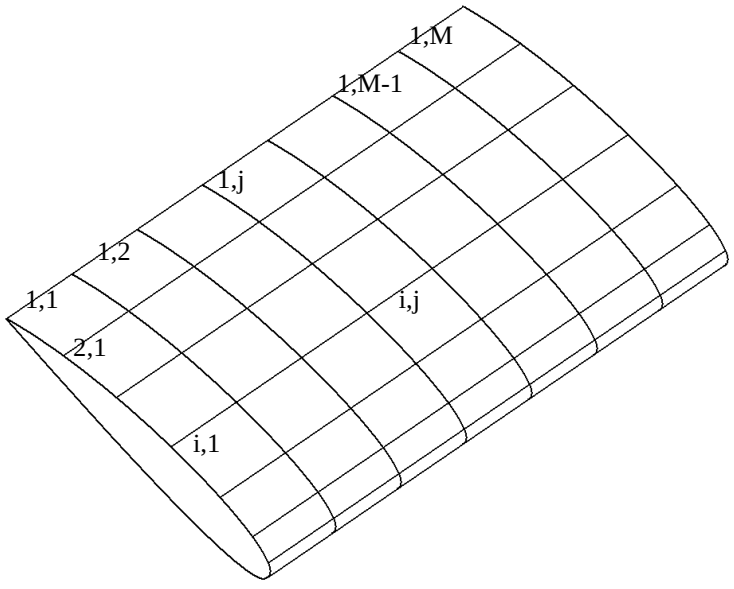

Figure 3-2 Panel indexing

Diagonal cross product will give vector collinear with the normal vector and dividing the product of diagonal vector with its absolute value will give the normal unit vector **n** of the panel (Figure 3-3).

Calculation of collocation point **c** is done by mean values of the panel vortex coordinates:

$$c_x = \frac{(x_1 + x_2 + x_3 + x_4)}{4},\ c_y = \frac{(y_1 + y_2 + y_3 + y_4)}{4},\ c_z = \frac{(z_1 + z_2 + z_3 + z_4)}{4} \qquad (3.2)$$

Where c_x, c_y, c_z are coordinates of collocation point of the panel, and x_1, y_1, z_1 to $x_4 y_4 z_4$ are coordinates of panel vertices.

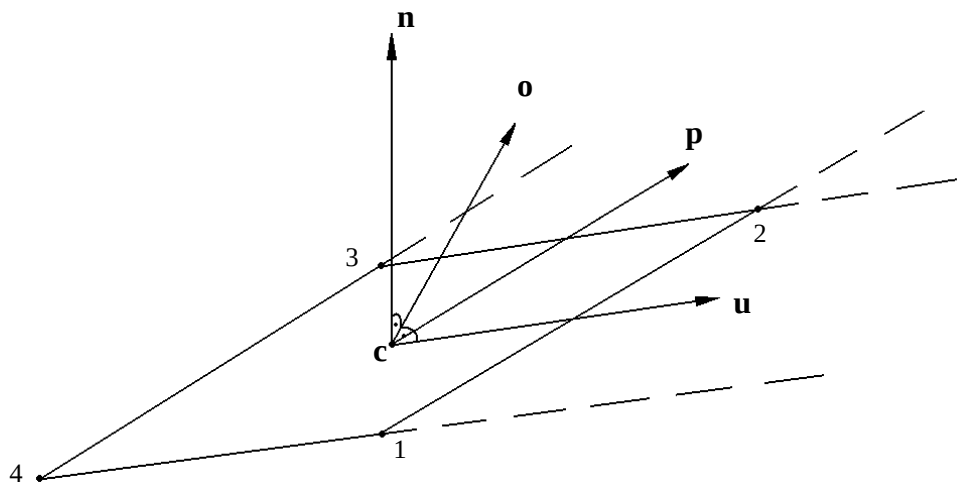

Figure 3-3 Collocation point and unit vectors of panel

It would be desired that collocation point coincides with center of gravity. Prior expression (3.2) gives the components of the vector of collocation points equal to the center of gravity for the rectangular panel, while the triangular panel deviates most from the center of gravity. This deviation from the center of gravity creates a negligible error.

Later in the program will be required (in addition to the unit normal) unit vectors in the longitudinal **u** and transverse **p** direction of the panel and the unit vector perpendicular to the unit vectors **n** and **u** - unit vector **o** (Figure 3-3). Calculation of the unit vectors in longitudinal and transverse direction is performed by:

$$u_x = \frac{(x_1 + x_2 - x_3 - x_4)}{2}, u_y = \frac{(y_1 + y_2 - y_3 - y_4)}{2}, u_z = \frac{(z_1 + z_2 - z_3 - z_4)}{2} \tag{3.3}$$

$$p_x = \frac{(x_2 + x_3 - x_4 - x_1)}{2}, p_y = \frac{(y_2 + y_3 - y_4 - y_1)}{2}, \; p_z = \frac{(z_2 + z_3 - z_4 - z_1)}{2}$$

Calculation of the unit vector perpendicular to the unit vectors $\mathbf{n}$ and $\mathbf{u}$ is done by

$$\mathbf{o} = \mathbf{n} \times \mathbf{u} \tag{3.4}$$

In 2D problems Kutta condition is added in a way that at the trailing edge vortex is added, whose intensity is equal to the difference in intensity of the top and bottom vortices at the airfoil trailing edge. In three-dimensional case, at the wing trailing edge (or other lifting surfaces) panel is added that extends from the trailing edge to some "far away" distance behind the aircraft with intensity equal to the difference in the intensity of upper vortex ring and lower surface ring at the trailing edge. This is easily done by adding predefined distance to the trailing edge point in x direction.

For purpose of calculating influence coefficients it will be necessary to transform panel vertex coordinates of influencing (one that affects) and collocation point coordinates of influenced (one that is affected) panel in the local coordinate system. Panel vertex coordinates (Figure 3-3) are calculated before calculating influence coefficients:

$$\begin{bmatrix} x \\ y \\ 0 \end{bmatrix}_{\text{lok}} = \begin{bmatrix} u_1 & u_2 & u_3 \\ o_1 & o_2 & o_3 \\ 0 & 0 & 0 \end{bmatrix} \begin{bmatrix} x \\ y \\ z \end{bmatrix}_{\text{glob}} \tag{3.5}$$

Where $[x \quad y \quad 0]^{\text{T}}_{\text{lok}}$ is i panel vertex vector in local coordinate system with z component equal to zero, $[x \quad y \quad z]^{\text{T}}_{\text{glob}}$ same, but in global coordinate system and, u_1, u_2, u_3 and o_1, o_2, o_3 aforementioned unit vectors of panel.

3.2. Influence coefficients calculation

Before presenting equations for calculating influence coefficients, basic equation for solving potential flow is showed:

$$\sum_{i=1}^{O} a_i \mu_i + \sum_{i=1}^{O} b_i \sigma_i = 0 \tag{3.6}$$

In expression (3.6) Dirichlet boundary condition is contained which says that potential within the body (or surface) equals zero. Defining constant potential within body is equivalent to Neumann boundary condition – zero flow on body surface with the difference that in this case only one equation is calculated; equation for potential, while in case of Neumann boundary condition it is necessary to calculate three velocity components.

Since 3D panel method program consists of a quadrilateral panels with constant distribution of sources and dipoles (quadrilateral dipole is equivalent to vortex ring) next are terms for potential of an arbitrary quadrilateral panel to an arbitrary point in space. The coordinate system is local, previously showed.

Constant source:

$$\begin{aligned}
\Phi = \frac{-\sigma}{4\pi}\Bigg\{\Bigg[& \frac{(x-x_1)(y_2-y_1)-(y-y_1)(x_2-x_1)}{d_{12}} \ln\frac{r_1+r_2+d_{12}}{r_1+r_2-d_{12}} \\
& + \frac{(x-x_2)(y_3-y_2)-(y-y_2)(x_3-x_2)}{d_{23}} \ln\frac{r_2+r_3+d_{23}}{r_2+r_3-d_{23}} \\
& + \frac{(x-x_3)(y_4-y_3)-(y-y_3)(x_4-x_3)}{d_{34}} \ln\frac{r_3+r_4+d_{34}}{r_3+r_4-d_{34}} \\
& + \frac{(x-x_4)(y_1-y_4)-(y-y_4)(x_1-x_4)}{d_{41}} \ln\frac{r_4+r_1+d_{41}}{r_4+r_1-d_{41}}\Bigg] \\
& - |z|\Bigg[\tan^{-1}\left(\frac{m_{12}e_1-h_1}{zr_1}\right) - \tan^{-1}\left(\frac{m_{12}e_2-h_2}{zr_2}\right) \\
& + \tan^{-1}\left(\frac{m_{23}e_2-h_2}{zr_2}\right) - \tan^{-1}\left(\frac{m_{23}e_3-h_3}{zr_3}\right) \\
& + \tan^{-1}\left(\frac{m_{34}e_3-h_3}{zr_3}\right) - \tan^{-1}\left(\frac{m_{34}e_4-h_4}{zr_4}\right) \\
& + \tan^{-1}\left(\frac{m_{41}e_4-h_4}{zr_4}\right) - \tan^{-1}\left(\frac{m_{41}e_1-h_1}{zr_1}\right)\Bigg]\Bigg\}
\end{aligned} \tag{3.7}$$

Constant dipole:

$$\Phi = \frac{\mu}{4\pi}\left[\tan^{-1}\left(\frac{m_{12}e_1 - h_1}{zr_1}\right) - \tan^{-1}\left(\frac{m_{12}e_2 - h_2}{zr_2}\right)\right.$$
$$+ \tan^{-1}\left(\frac{m_{23}e_2 - h_2}{zr_2}\right) - \tan^{-1}\left(\frac{m_{23}e_3 - h_3}{zr_3}\right)$$
$$+ \tan^{-1}\left(\frac{m_{34}e_3 - h_3}{zr_3}\right) - \tan^{-1}\left(\frac{m_{34}e_4 - h_4}{zr_4}\right) \qquad (3.8)$$
$$\left.+ \tan^{-1}\left(\frac{m_{41}e_4 - h_4}{zr_4}\right) - \tan^{-1}\left(\frac{m_{41}e_1 - h_1}{zr_1}\right)\right]$$

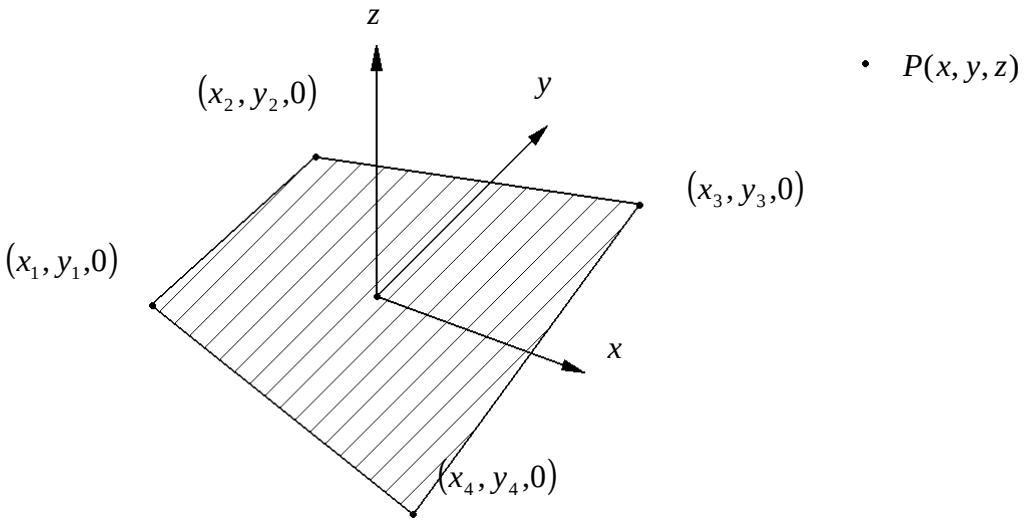

Figure 3-4 Quadrilateral panel

Where, according to Figure (3-4), $x_1 - x_4, y_1 - y_4, z_1 - z_4$ are panel vertex coordinates, x, y, z coordinates of influenced point, σ and μ sources and dipoles strengths, and the following values are:

$$m_{12} = \frac{y_2 - y_1}{x_2 - x_1}, m_{23} = \frac{y_3 - y_2}{x_3 - x_2}, m_{34} = \frac{y_4 - y_3}{x_4 - x_3}, m_{41} = \frac{y_1 - y_4}{x_1 - x_4}$$

$$r_k = \sqrt{(x - x_k)^2 + (y - y_k)^2 + z^2}\ ,\ k = 1,2,3,4$$

$$e_k = (x - x_k)^2 + z^2,\ k = 1,2,3,4$$

$$h_k = (x - x_k)(y - y_k),\ k = 1,2,3,4$$

Expressions (3.7) and (3.8) are results of integration of constant sources and dipoles on surface of arbitrary quadrilateral panel and are listed in [1]. In case of a triangular panel

(quadrilateral with a pair of adjacent vertices of equal coordinates) raw in the equations relating to the side whose length is equal to zero is zero (this is handled by a simple "if" loop to avoid dividing by zero).

Influence of a constant dipole on collocation point of that very same panel is 0.5.

Following discussion regarding the influence coefficients, very essential to accelerating program, is replacement of a quadrilateral panel with a constant distribution of sources and/or dipoles with point source and/or dipole in space. This will make sense if influenced point is far enough from the influence panel (result convergence when considering this distance is performed in chapter 4).

Equations (3.9) and (3.10) represent potential of a point source and doublet on point at x, y and z.

$$\Phi(x,y,z) = \frac{-\sigma S}{4\pi\sqrt{x^2+y^2+z^2}} \tag{3.9}$$

$$\Phi(x,y,z) = \frac{-\mu S}{4\pi} z\left[x^2+y^2+z^2\right]^{-3/2} \tag{3.10}$$

where S is panel surface.

Local coordinate system is defined so that in case of a dipole it is oriented at positive direction of axis z. Of course in the case of the source, choice of coordinate system is not essential, but since coordinates in local coordinate system are already calculated they will be used.

In all previous expressions for the potential, the strength of the source and dipole σ and μ appears. Since these values in this part of the program are the wanted values, for now they are set to 1 and are actually expressions for calculating the influence coefficients.

In order to make the solution uniquely defined, right combination of sources and dipoles must be selected. Setting up sources to:

$$\sigma_i = \mathbf{n}_i \cdot \mathbf{V}_\infty \tag{3.11}$$

where $\mathbf{V}_\infty$ is vector of free stream velocity, will result in the value of the dipole μ as unknowns. Reason for placing sources at this value lies in fact that for non-lifting case this combination of sources will take over most of normal flow on walls, and therefore making strengths of dipoles less in value which represents a certain numerical advantage [1].

Assembling matrix of influence coefficients and "right hand side" vector in which is included boundary condition enables solving system of equations whose solution is precisely strengths of dipoles. System of equations looks like:

$$\begin{bmatrix} a_{11} & a_{12} & \dots & a_{1O} \\ a_{21} & a_{22} & \dots & a_{2O} \\ \vdots & \vdots & \ddots & \vdots \\ a_{O1} & a_{O2} & \dots & a_{OO} \end{bmatrix} \begin{bmatrix} \mu_1 \\ \mu_2 \\ \vdots \\ \mu_O \end{bmatrix} = - \begin{bmatrix} b_{11} & b_{12} & \dots & b_{1O} \\ b_{21} & b_{22} & \dots & b_{2O} \\ \vdots & \vdots & \ddots & \vdots \\ b_{O1} & b_{O2} & \dots & b_{OO} \end{bmatrix} \begin{bmatrix} \sigma_1 \\ \sigma_2 \\ \vdots \\ \sigma_O \end{bmatrix} \tag{3.12}$$

where O is number of panels, **a** matrix of dipole influence coefficients **b** matrix of source influence coefficients.

Since on the right side of equation (3.12) are known values, they can be multiplied into vector which is called $\mathbf{c}_{\mathrm{RHS}}$ (right hand side).

$$\begin{bmatrix} a_{11} & a_{12} & \dots & a_{1O} \\ a_{21} & a_{22} & \dots & a_{2O} \\ \vdots & \vdots & \ddots & \vdots \\ a_{O1} & a_{O2} & \dots & a_{OO} \end{bmatrix} \begin{bmatrix} \mu_1 \\ \mu_2 \\ \vdots \\ \mu_O \end{bmatrix} = \begin{bmatrix} c_{\mathrm{RHS}1} \\ c_{\mathrm{RHS}2} \\ \vdots \\ c_{\mathrm{RHS}O} \end{bmatrix} \tag{3.13}$$

or simply

$$\mathbf{a} \cdot \boldsymbol{\mu} = \mathbf{c}_{\mathrm{RHS}} \tag{3.14}$$

It follows:

$$\boldsymbol{\mu} = \mathbf{a}^{-1} \cdot \mathbf{c}_{\mathrm{RHS}} \tag{3.15}$$

On lifting components on which lift should be calculated and thus induced drag, a three-dimensional equivalent of Kutta condition is applied. In this case it is the panel with continuous distribution of dipoles (vortex rings) whose strength corresponds to difference in strengths of upper and lower panels on trailing edge, and spreads from trailing edge downstream by predefined value (Figure 3-5).

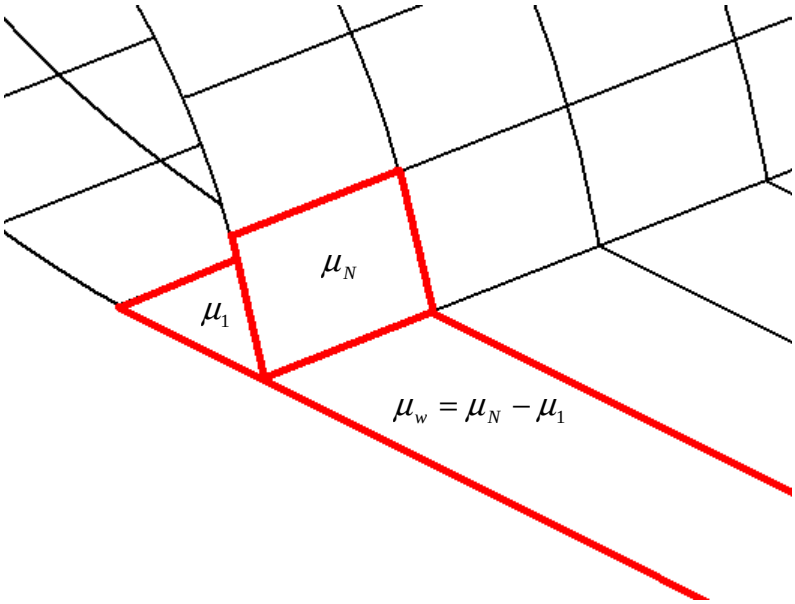

Figure 3-5 Kutta condition on trailing edge of the wing

Since the newly introduced variable depends on the two existing (strength of the panels above and below the trailing edge), only matrix of influence coefficients is modified so that the panel's influence coefficient on trailing edge is added or subtracted by influence coefficient of wake panel, depending on whether the panel is on top or bottom of the edge (3.16).

$$(a_{11} - a_{1w})\mu_1 + \cdots + a_{1i}\mu_i + \cdots (a_{1N} + a_{1w})\mu_N + \sum_{j=1}^{N} b_{1j}\sigma_j = 0 \qquad (3.16)$$

In expression (3.16) only one row of panels per airfoil is being observed.

Assembling matrix of influence coefficients presents problems with speed and computation.

Since this is a double "for" loop (counter) which includes influential and influenced panels, or fourfold loop if we take into account chordwise and spanwise counter, calculation time is very long. Introduction of "far field" point singularities significantly accelerates calculation and this will be shown in chapter four at convergence of results with varying "far field" parameter.

Furthermore, the matrix of influence coefficients **a** and **b** consists of $O \times O$ elements, where O is the total number of panels, and therefore occupies a large portion of computer memory. For ~10000 elements, each matrix takes ~1 GB. In case of lack of computer memory, it is suitable in Matlab to convert these matrices to "single" precision since impact on accuracy is negligible. This reduces size of matrix to their half.

3.3. Solution of system of equations

Once a matrix of influence coefficients is assembled and RHS (right hand side vector) has been calculated, strengths of dipole $\boldsymbol{\mu}$ can be calculated. Typically, process involves inverting matrix of influence coefficients and its multiplication with a RHS. Matlab as an engineering program has a predefined and optimized function for this operation.

The solution of system of equations is, along with calculating influence coefficients, also time and resource consuming. Time of calculation cannot be reduced since the Matlab is already optimized, but it is possible to free up memory of unneeded variables like a matrix of influence coefficients $\mathbf{b}$ which is already used to create RHS part of the equation.

3.4. Calculation of velocity, pressure and forces

After dipole strengths have been calculated, calculation of velocity, pressure and forces can be made.

Velocity components are calculated by:

$$q_u = -\frac{\partial \mu}{\partial u},\ q_p = -\frac{\partial \mu}{\partial p} \tag{3.17}$$

which says that induced velocity is equal to local change of potential in observed direction. In this case this is the strength of dipole in longitudinal and transverse panel direction.

The usual method is (central difference method):

$$q_u = \frac{\mu_{i-1} - \mu_{i+1}}{\Delta u} \tag{3.18}$$

and says that induced velocity in direction **u** (direction of propagation of longitudinal panel) is equal to difference in strengths of dipole in front of and behind the observed panel divided by distance of collocation points of panel in front and behind observed panel.

In this case, method is used which will interpolate dipole strengths into second order curve using three points and find curve slope in observed point. Method is performed using command "polyfit" in Matlab, which finds three second order polynomial coefficients and the required value (slope) is exactly second coefficient.

In order to convert speed from local coordinate system to global, first vector of transverse induced velocity (not necessarily perpendicular to the longitudinal panel distribution) must be converted to the perpendicular induced velocity (perpendicular to the longitudinal and normal unit vector).

$$q_o = (\mathbf{p} \cdot \mathbf{o}) q_p \tag{3.19}$$

Where **p** and **o** are transverse and vertical unit vectors (section 3.1), and q_p and q_o transverse and perpendicular induced velocities.

Velocity components of free stream converted to local coordinate system are:

$$g_u = \mathbf{u} \cdot \mathbf{V}_\infty,\ g_o = \mathbf{o} \cdot \mathbf{V}_\infty \tag{3.20}$$

where g_u and g_o are velocity components of free stream in local coordinate system, $\mathbf{V}_\infty$ velocity vector of free stream, and **u** and **o** longitudinal and perpendicular unit vectors of observed panel. Induced velocities and free stream velocity are added up to get the total velocity:

$$\begin{bmatrix} v_x \\ v_y \\ v_z \end{bmatrix} = \begin{bmatrix} u_x & o_x \\ u_y & o_y \\ u_z & o_z \end{bmatrix} \begin{bmatrix} (g_u - q_u) & (g_o - q_o) \end{bmatrix} \tag{3.21}$$

From velocity field, pressure field is calculated using Euler - Bernoulli equation:

$$c_p = 1 - \frac{\sqrt{v_x^2 + v_y^2 + v_z^2}}{V_\infty^2} \tag{3.22}$$

From pressure field forces and moments are calculated by:

$$F_i = -\sum_{k=1}^{O} c_{p_k} S_k n_{ik} q \tag{3.23}$$

where F_i is force in i direction, S_k panel surface, n_{ik} i component normal unit vector, O number of panels and q reference (dynamic) pressure,

$$\begin{aligned} M_l &= \sum_{i=1}^{O} c_{p_i} S_i n_{y_i} q c_{z_i} - \sum_{i=1}^{O} c_{p_i} S_i n_{z_i} q c_{y_i} \\ M_m &= -\sum_{i=1}^{O} c_{p_i} S_i n_{x_i} q c_{z_i} + \sum_{i=1}^{O} c_{p_i} S_i n_{z_i} q c_{x_i} \\ M_n &= \sum_{i=1}^{O} c_{p_i} S_i n_{x_i} q c_{y_i} - \sum_{i=1}^{O} c_{p_i} S_i n_{y_i} q c_{x_i} \end{aligned} \tag{3.24}$$

where M_l, M_m and M_n are rolling (about the longitudinal axis – x), pitching (about the transverse axis – y) and yaw moment (about the vertical axis – z), a c_x, c_y and c_z coordinates of the collocation points of the observed panel.

4. OVERVIEW OF 3D PANEL METHOD RESULTS

In this chapter, the results of 3D panel method analysis are evaluated.

First what should be done is to analyze convergence of results with respect to density of panels. Thus an insight into program behavior is obtained and optimal mesh density determined.

Next is analysis of results convergence with respect to "far field" coefficient, where optimal value of coefficient is obtained.

Finally, accuracy of program is analyzed with comparison to numerical program FLUENT where FLUENT also will be analyzed for the convergence of solutions in order to select the optimal mesh density.

4.1. Analysis of convergence of solutions with respect to mesh density

For sensitivity analysis of mesh, a wing of the following characteristics will be used (Figure 4-1):

Wing span	- 5 m
Root chord length	- 1 m
Tip chord length	- 0.3 m
Tip incidence angle	- -3°
Quarter wing sweep	- 30°
Angle of attack	- 2°
Airfoil	- NACA 65-415

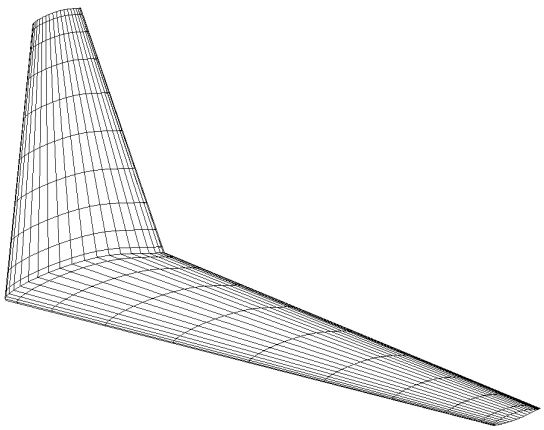

Figure 4-1 Geometry of the analyzed wing

Due to required higher density of mesh at leading and trailing edge as well as root and tip of wing, cosine distribution is used. Airfoil file is generated with external program The NACA Airfoil Ordinate Generation Program v4.5.

Out of generated data, most interesting will be coefficients of vertical force (C_Z), longitudinal force (C_X) and torque about the y-axis - pitching moment (C_m).

4.1.1. Convergence vs. number of panels per wingspan

Analysis is performed for a series of panel numbers (M) per wingspan (including both halves of wings):

$M = [4, 8, 12, 16, 20, 24, 28, 32, 36, 40, 44, 48, 52, 56, 60]$

Number of panels per airfoil in each case was 40.

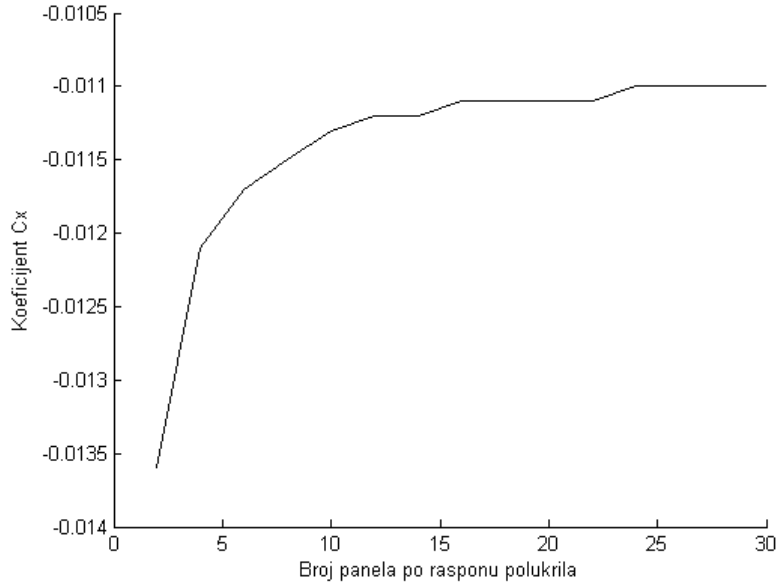

Diagram 4-1 Longitudinal force coefficient vs. half wing panel number

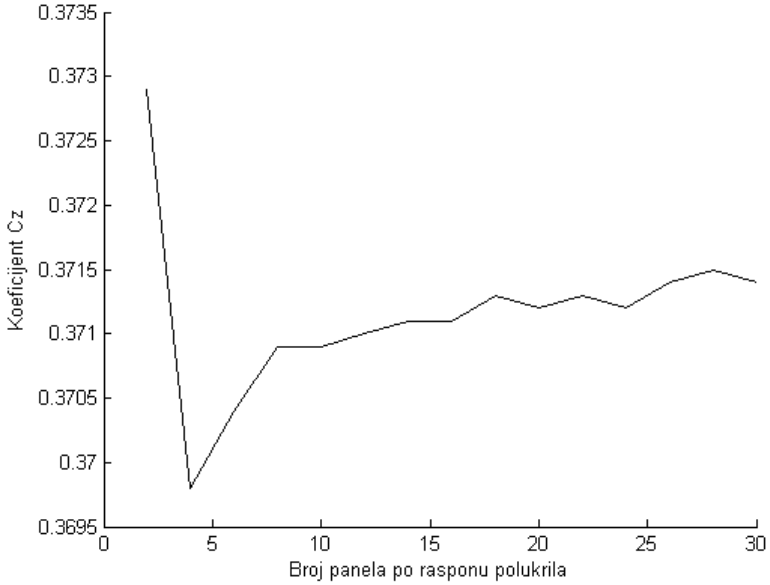

Diagram 4-2 Vertical force coefficient vs. half wing panel number

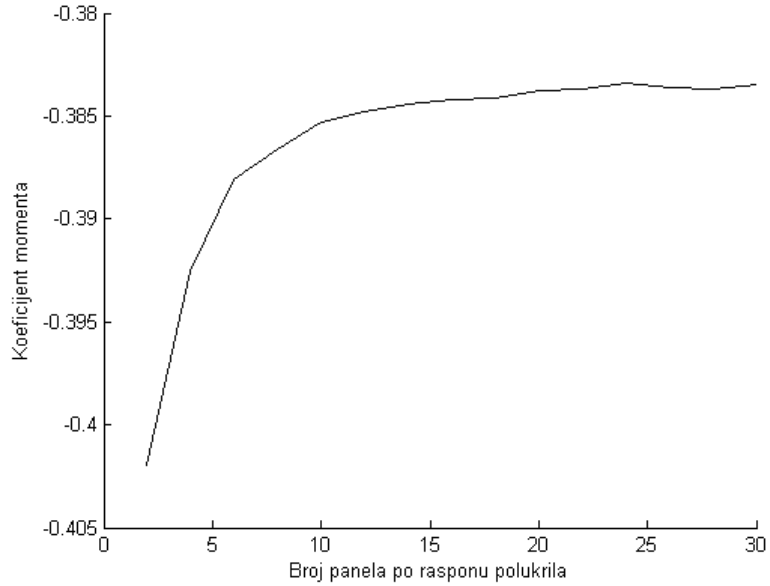

Diagram 4-3 Pitching moment coefficient vs. half wing panel number

From the previous diagrams, convergence of results is apparent, lower for forcer, higher for torque. Based on convergence of views, three different density geometries for different purposes are chosen:

1) Coarse mesh of 10 panels by wingspan. It will give a very quick solution with little accuracy. Such mesh is suitable for high-speed calculations such as in the preliminary design or in some tests that do not require higher accuracy.
2) Optimal mesh of 20 panels per wingspan. This mesh gives best results if observing ratio of accuracy and speed.
3) Finally, the finest mesh of 40 panels per wingspan that makes sense to use only for very fine calculations.

4.1.2. Convergence vs. number of panels per wing airfoil

Analysis is performed for a series of panel numbers (N) per airfoil:

$N = [10, 20, 30, 40, 50, 60, 70, 80, 90, 100]$

In each case number of panels per wingspan was 20.

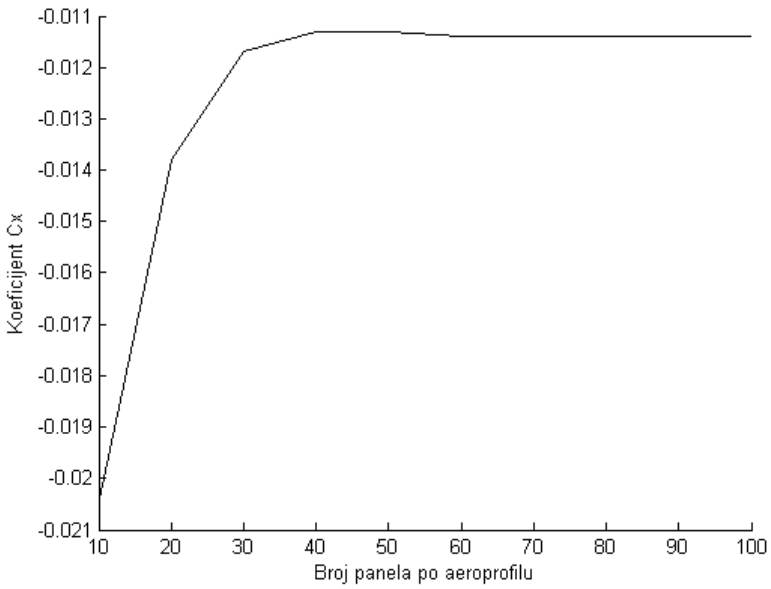

Diagram 4-4 Longitudinal force coefficient vs. airfoil panel number

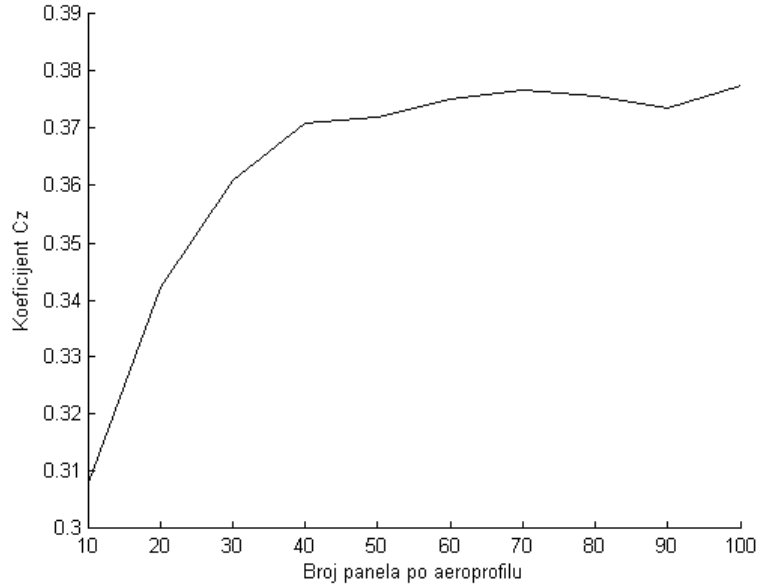

Diagram 4-5 Vertical force coefficient vs. airfoil panel number

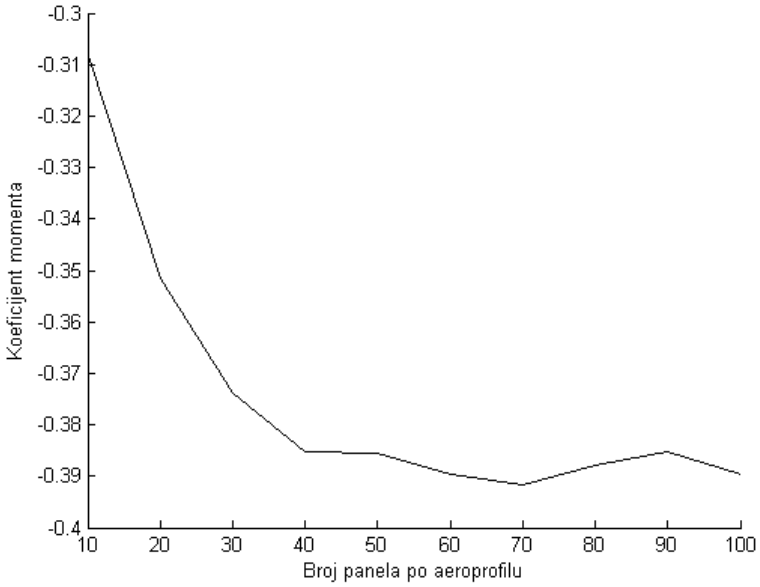

Diagram 4-6 Pitching moment coefficient vs. airfoil panel number

Three mesh densities are selected; coarse of 24, optimum of 40 and a fine mesh of 60 panels per airfoil.

Based on previously selected mesh densities, three wing meshes are prepared; coarse, optimal and fine (Figure 4-2):

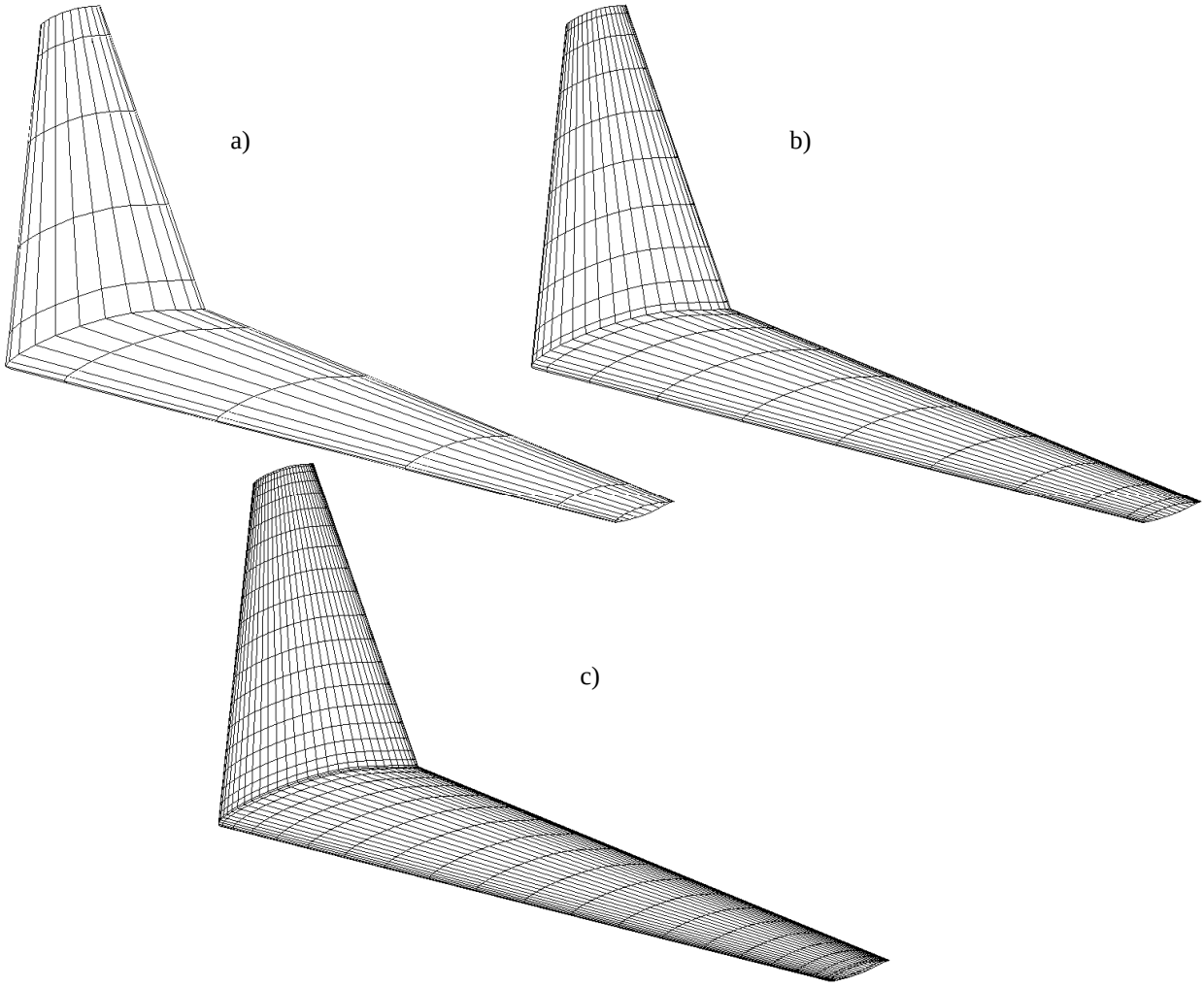

Figure 4-2 a) coarse, b) optimal and c) fine wing mesh

Following diagram shows similarity in chordwise pressure coefficient at mid-span of half wing for three different meshes:

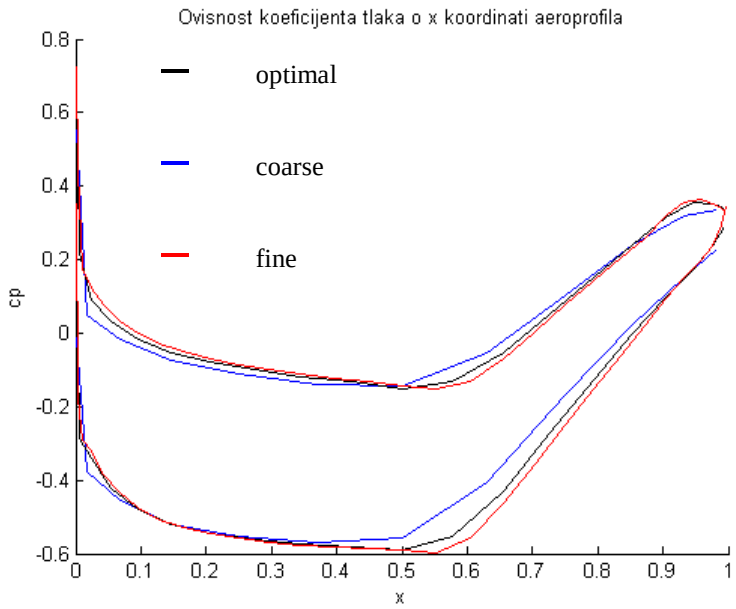

Diagram 4-7 Pressure coefficient for coarse (blue), optimal (black) and fine (red) wing

It is also interesting to compare computation times in seconds (Figure 4-8). Significant increase in computation time can be seen for fine grid which prevents its wider application.

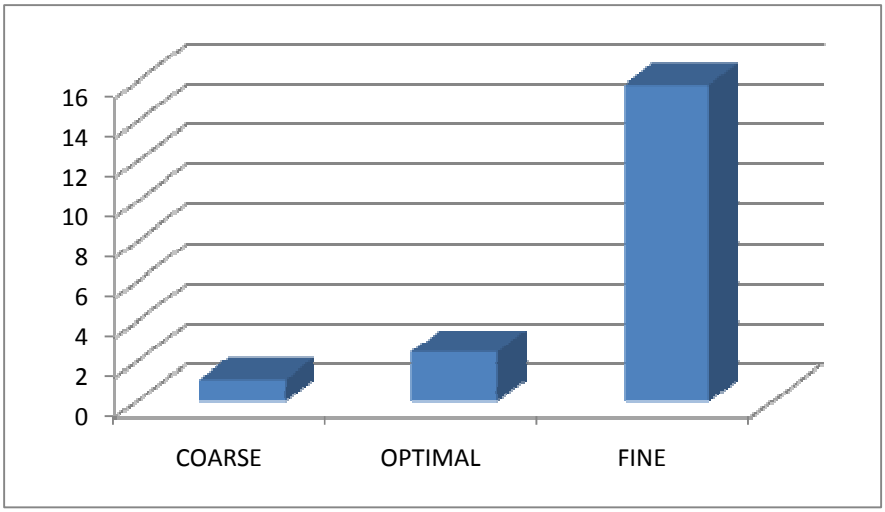

Diagram 4-8 Computation time vs. mesh density

4.2. Results of 3D panel method and FLUENT for aircraft configuration.

4.2.1. Description of selected configuration

In order to evaluate 3D panel method program, aircraft configuration was chosen that will be analyzed in 3D panel method and in FLUENT (Table 4-1). The aircraft is conventional configuration with middle wing position, swept wing and T-tail (Figure 4-4).

aircraft length	45,69	m
wing span	42,40	m
aircraft height	12,91	m
wing area (reference)	111,00	m²
wing root chord length	7,35	m
wing tip chord length	2,60	m
mean aerodynamic chord	6,00	m
wing sweep	15,50	°
wing dihedral	-4,65	°
angle of geometric twist	-2,00	°
root airfoil	NACA 65415	
tip airfoil	NACA 65015	
wing aspect ratio (AR)	8,52	
fuselage width	6,00	m
fuselage height	5,00	m
vertical stabilizer height	7,59	m
vertical stabilizer root chord length	6,65	m
vertical stabilizer tip chord length	5,29	m
vertical stabilizer sweep	33,00	°
vertical stabilizer airfoil	NACA 65012	
horizontal stabilizer root chord length	5,29	m
horizontal stabilizer tip chord length	2,18	m
horizontal stabilizer span	19,12	m
horizontal stabilizer sweep	32,00	°
horizontal stabilizer airfoil	NACA 65012	

Table 4-1 Geometric characteristics of selected aircraft configuration

Figure 4-3 Three projections of selected aircraft configuration

The selected configuration is similar to configuration of modern turboprop A400M Airbus military transporter with the difference that wing is moved from high to the middle position relative to the fuselage.

4.2.2. Geometry discretization for panel method

Based on convergence results performed previously, three meshes are prepared; coarse - 1554 elements, optimum - 4732 elements and fine - 11288 elements (Figure 4-4).

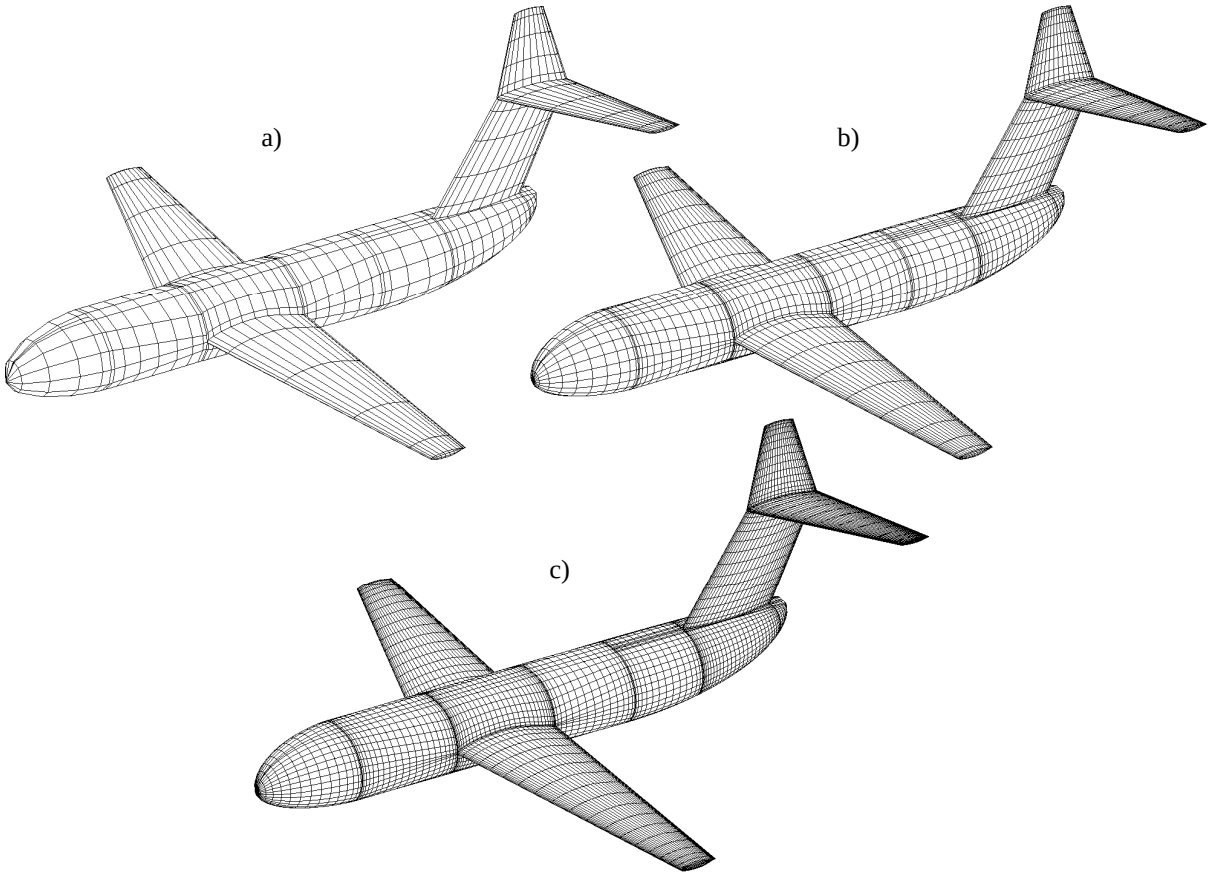

Figure 4-4 Three meshes: a) coarse b) optimal and c) fine

The basic characteristic is that mesh is composed of a series of surfaces in 3D space, using cosine distribution to accomplish higher density at the edges of panel surfaces.

In this case, optimal mesh will be used (Figure 4-4b).

4.2.3. Convergence of solution with respect to ''far field'' coefficient

As explained in the third chapter, if influenced panel is far away from influential, rectangular panel is replaced with point singularity in space. The distance at which this will occur is "far field" coefficient multiplied with longer panel diagonal.

On diagrams 4-9 to 4-11 are visible coefficient convergences for optimal wing.

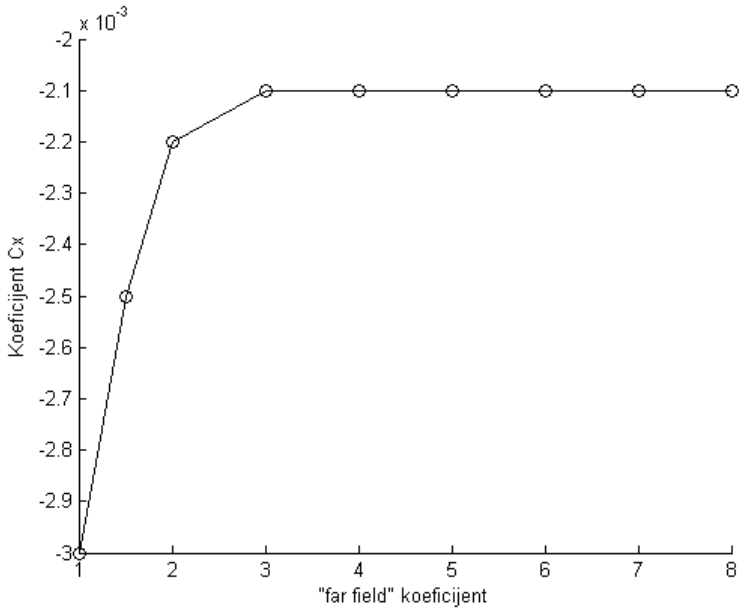

Diagram 4-9 Longitudinal force coefficient vs. ''far field'' coefficient

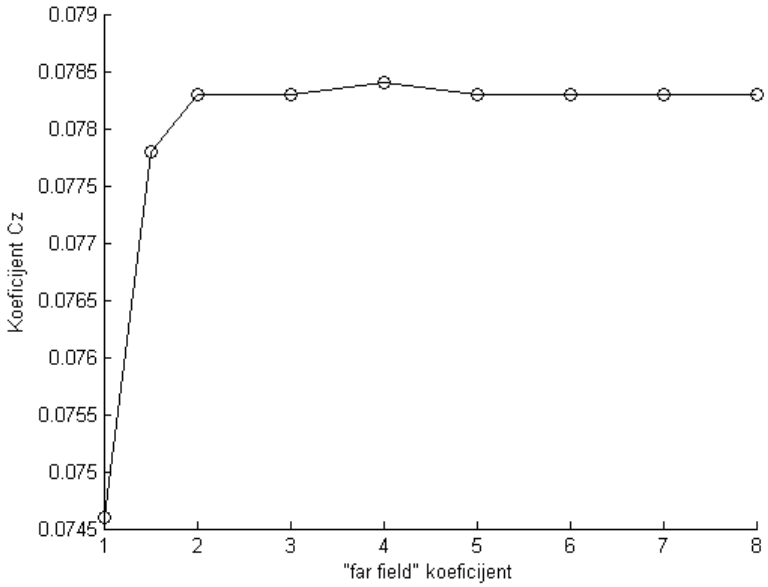

Diagram 4-10 Vertical force coefficient vs. ''far field'' coefficient

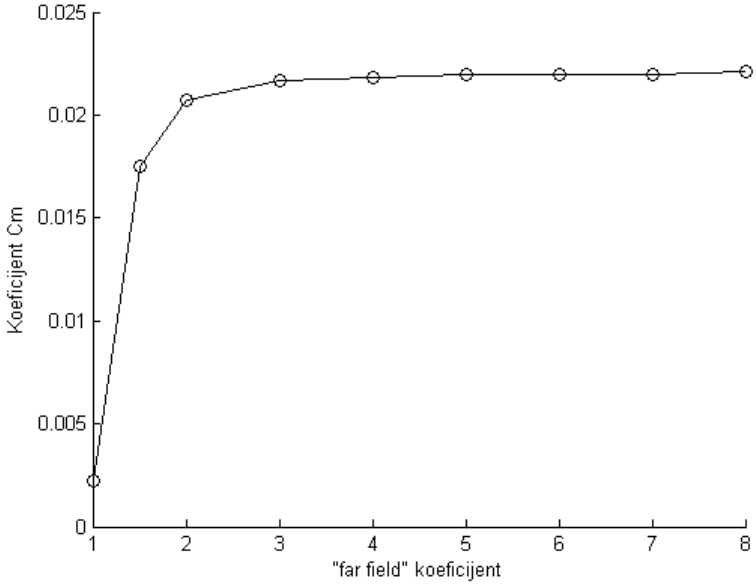

Diagram 4-11 Pitching moment coefficient vs. "far field" coefficient

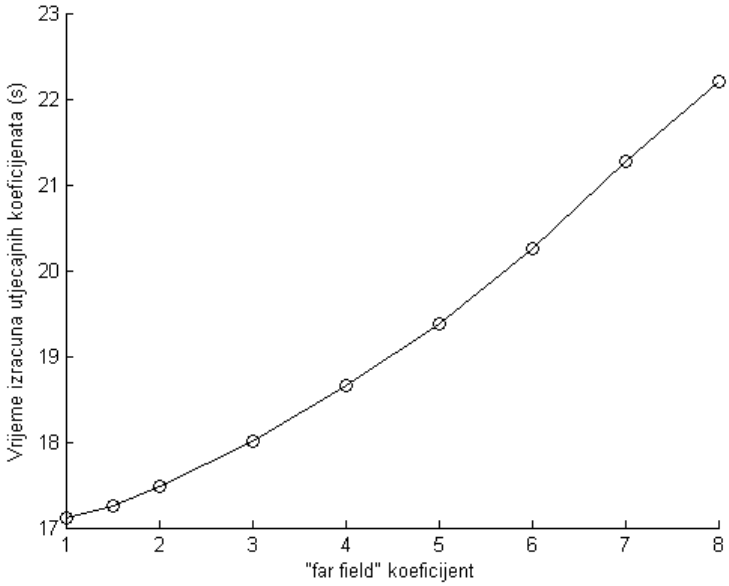

Diagram 4-12 Influence coefficients calculation time vs. "far field" coefficient

Based on previous convergence diagrams and diagram 4-12 showing influence coefficients calculation time, value of 5 for "far field" coefficient is chosen. For a fine grid of 11288 elements, calculation of influence coefficients is reduced from 244 seconds to 101 seconds, optimum of 4732 elements from 43 to 19 seconds, while for coarse of 1554 from 5 to 3 seconds. From this it is easy to conclude that influence coefficients calculation time is halved.

4.2.4. Discretizing aircraft geometry for FLUENT

Geometry discretization for FLUENT package is performed in its preprocessor GAMBIT. Unlike panel methods, where discretization is done only on surface, in finite volume methods (FVM) whole flow domain is discretized – volume surrounding aircraft. Since it is very important in FVM that surfaces that are enclosing flow domain are far away (unlike panel method, where choice of singularities fulfill "far field" boundary condition on their own), selected flow volume has dimensions 300x160x200m (Figure 4-5).

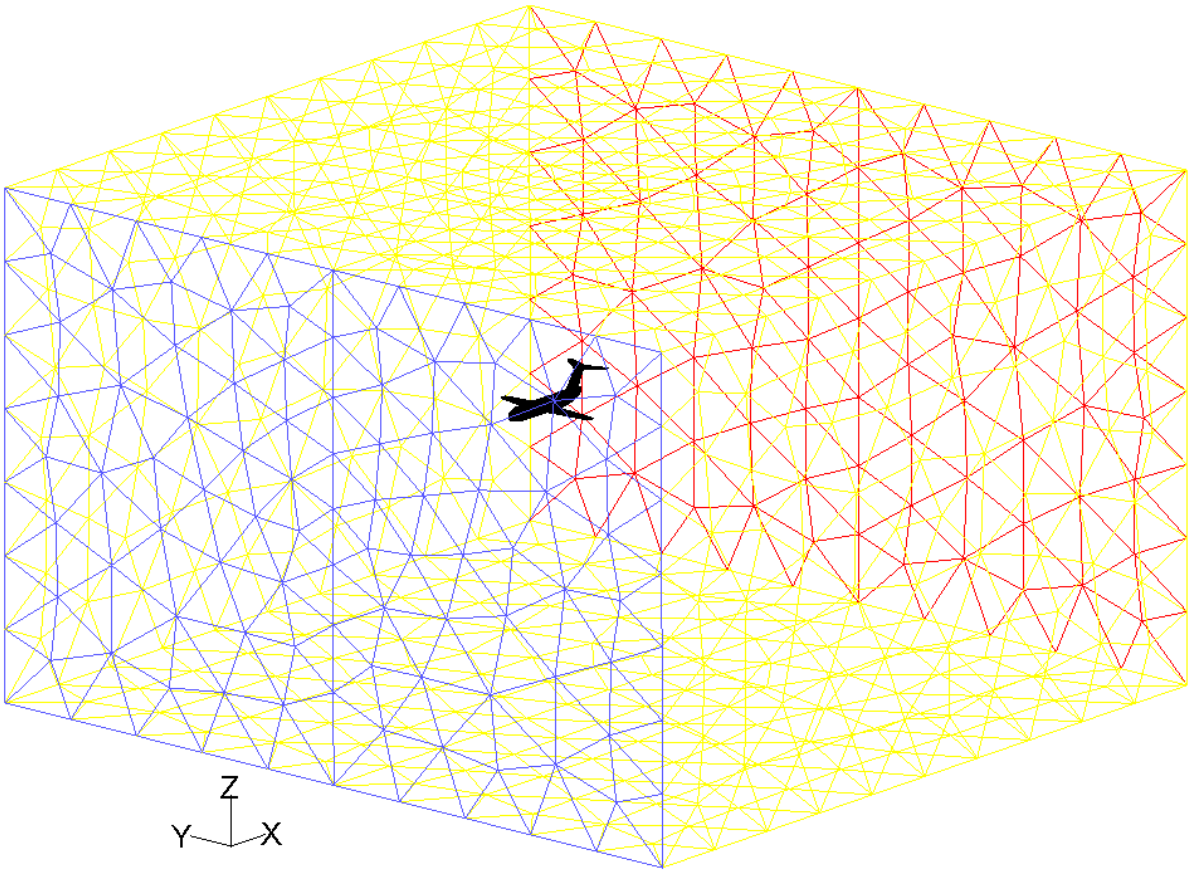

Figure 4-5 Flow domain in FLUENT

Since it is necessary to analyze convergence in FLUENT, 6 meshes of different densities have been generated (19410, 49254, 117998, 233400, 682299 and 2190454 elements). Mesh consists of triangular elements on surfaces and tetrahedral in flow volume. On following figures meshes on only half of vertical stabilizer are shown (due to differences in mesh density, it would not be possible to show whole mesh (Figure 4-6).

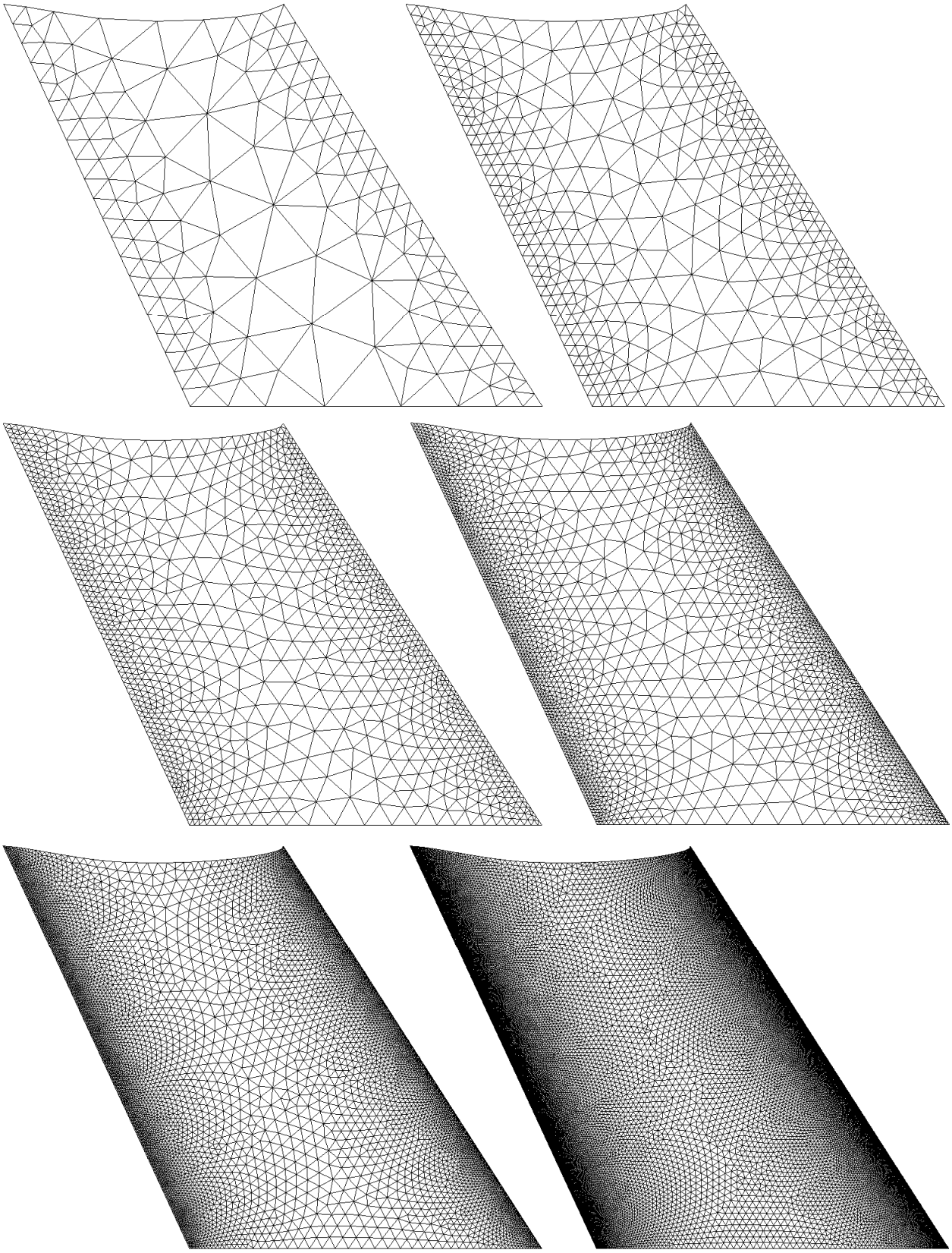

Figure 4-6 Different mesh densities for FLUENT analysis

After examining the convergence in FLUENT, one mesh will be selected for further work.

4.2.5. Convergence testing in FLUENT

Parameters and settings in FLUENT are standard (default) except for setting model to inviscid and setting pressure and momentum discretization to second order. By removing viscous properties we moved away from exact solution, but closer to potential flow. By setting second order discretization, accuracy of calculation in FLUENT is increased.

Calculation in FLUENT is iterative. Calculation can be automatically stopped when residuals drop to an appropriate level. In this case, solution will be let to converge completely since often aerodynamic coefficients are changing continuously as residuals.

Diagram (4-13) shows time required for complete convergence for different mesh densities. Since sizes have exponential growth, diagram is with logarithmic axes.

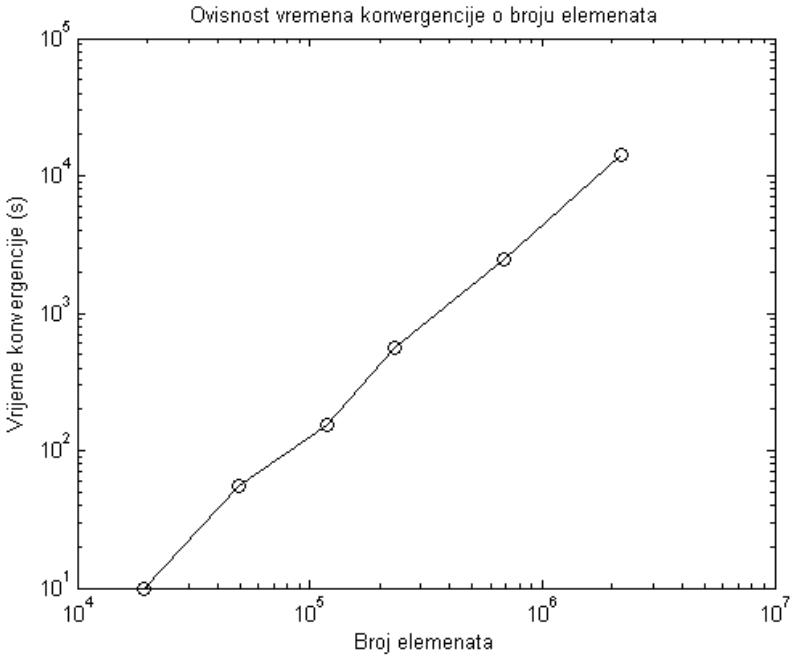

Diagram 4-13 Computation time in FLUENT vs. number of elements

Diagram (4-14) shows convergence results in form of aerodynamic force and moment coefficients (Cx-black, Cz-red and Cm-blue).

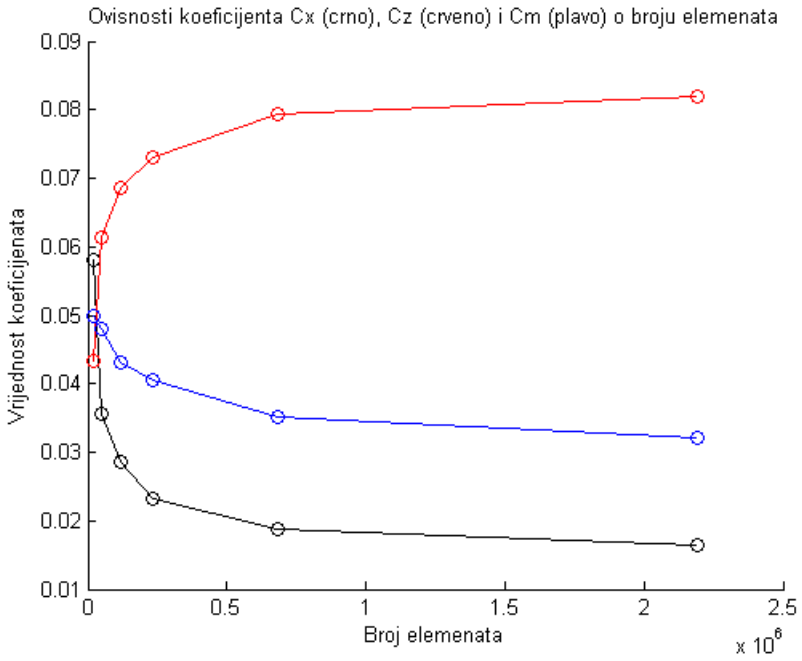

Diagram 4-14 Convergence results in FLUENT

Based on diagram (4-14), mesh of 233400 elements (Figure 4-7) was selected for further comparison. It is important to emphasize that the gradients such as lift gradient (vs. angle of attack) will be less sensitive to mesh fineness.

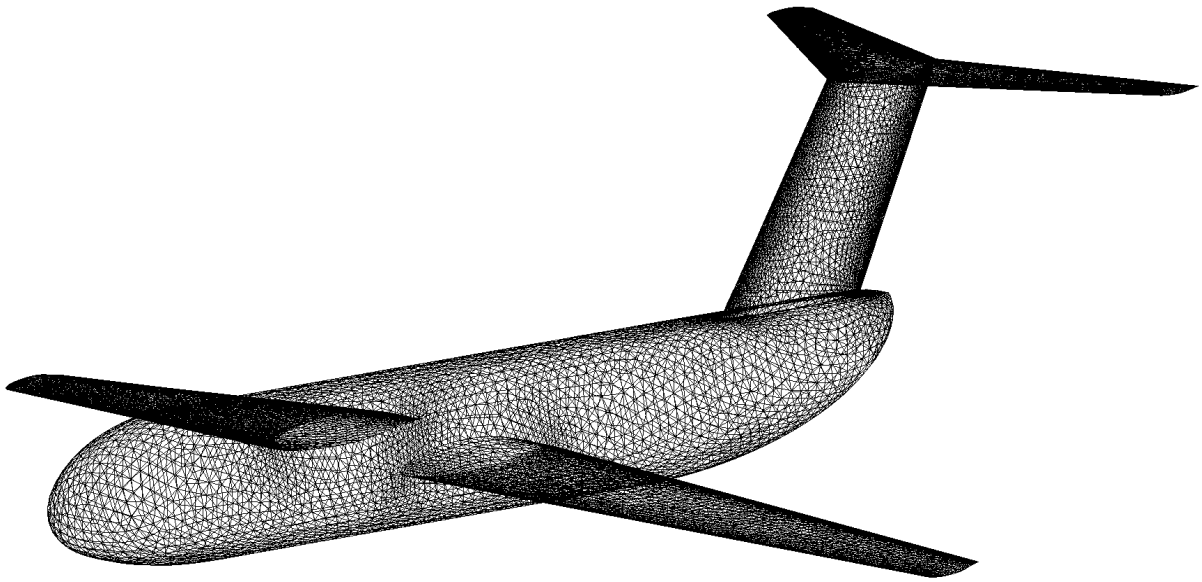

Figure 4-7 Selected FLUENT mesh

4.2.6. Comparison of results

The analysis was performed for range of angles of attack from -4 to 6 degrees with step of 2 degrees, and for sideslip angles 0 to 10 degrees with step of 2 degrees. Required values are shown in Table 4-2 along with symbols.

Value	Symbol
Lift coefficient at zero angle of attack	C_{L0}
Lift coefficient gradient	$C_{L\alpha}$
Drag coefficient at zero angle of attack	C_{D0}
Oswald coefficient	e
Pitching moment coefficient at zero angle of attack	C_{M0}
Pitching moment gradient	$C_{M\alpha}$
Lateral force coefficient gradient	$C_{Y\beta}$
Rolling moment coefficient gradient	$C_{l\beta}$
Yaw moment coefficient gradient	$C_{n\beta}$

Table 4-2 Aerodynamic coefficients used for comparison

Oswald coefficient e was calculated in Matlab:

$$e = \frac{180}{A\pi^2 K}$$

Where A is wing aspect ratio (ratio of square wing span and wing area) and K coefficient next to square of angle of attack:

$$C_D = C_{D0} + C_{D\alpha}\alpha + K\alpha^2$$

Usually, Oswald coefficient is obtained from the quadratic dependence of resistance to lift, but here is just important to compare quadratic behavior of resistance to angle of attack.

In the following table (Table 4-3) results are shown (in form of aerodynamic coefficients) and their difference in percentage.

aerodynamic coefficient	FLUENT	3D Panel Method	Difference (%)
C_{L0}	0.0725	0.0735	1
$C_{L\alpha}$	5.9915	5.7658	-4
C_{D0}	0.0231	-0.0020	/
e	0.8544	0.8737	2
C_{M0}	0.0471	0.0383	-23
$C_{M\alpha}$	-4.4899	-3.3574	-34
$C_{Y\beta}$	0.9351	0.8487	-10
$C_{l\beta}$	-0.0014	-0.0023	39
$C_{n\beta}$	0.2952	0.2705	-9

Table 4-3 Aerodynamic coefficients in FLUENT and 3D panel method

Good match is visible in lift coefficient in longitudinal analysis and lateral force and yaw moment gradients in lateral analysis.

As far as drag is concerned, Oswald coefficient shows good agreement of drag quadratic behavior. On the other hand, drag coefficient at zero angle of attack is incomparable.

Pitch moment coefficient has small difference in zero value and gradient.

Next are diagrams of forces and moments depending on their angles. FLUENT results are black, while 3D panel method results are colored blue.

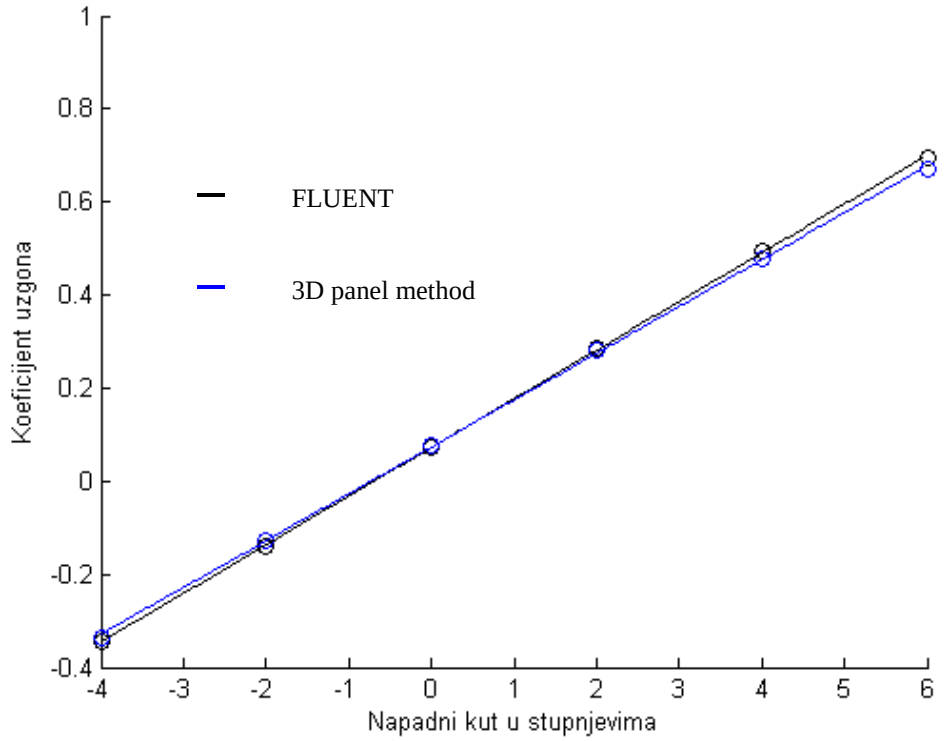

Diagram 4-15 Lift coefficient vs. angle of attack

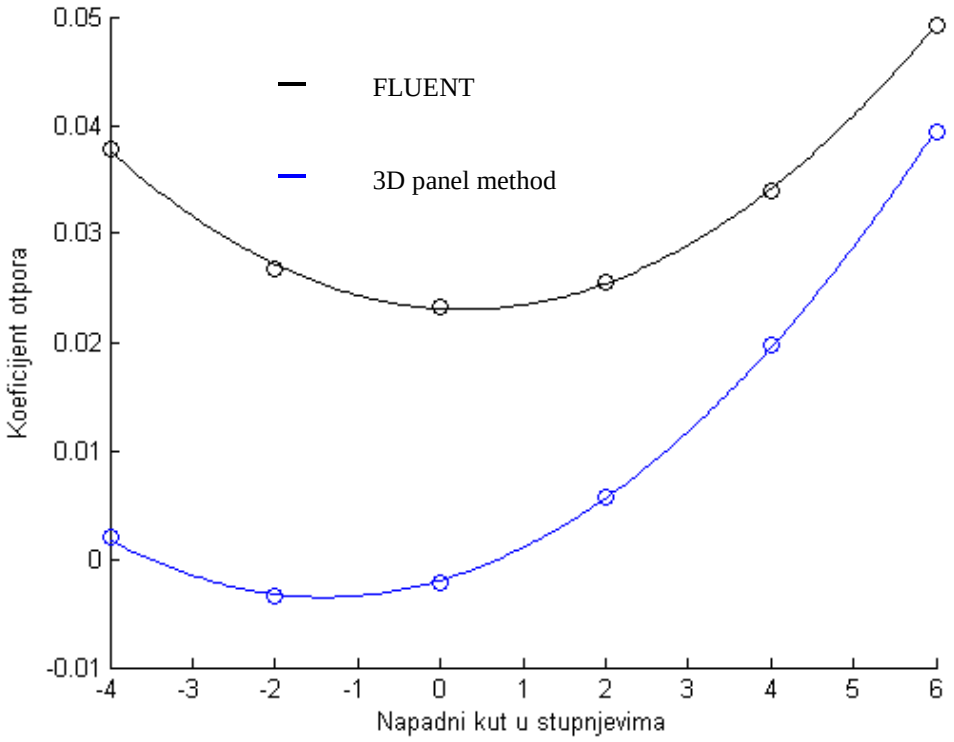

Diagram 4-16 Drag coefficient vs. angle of attack

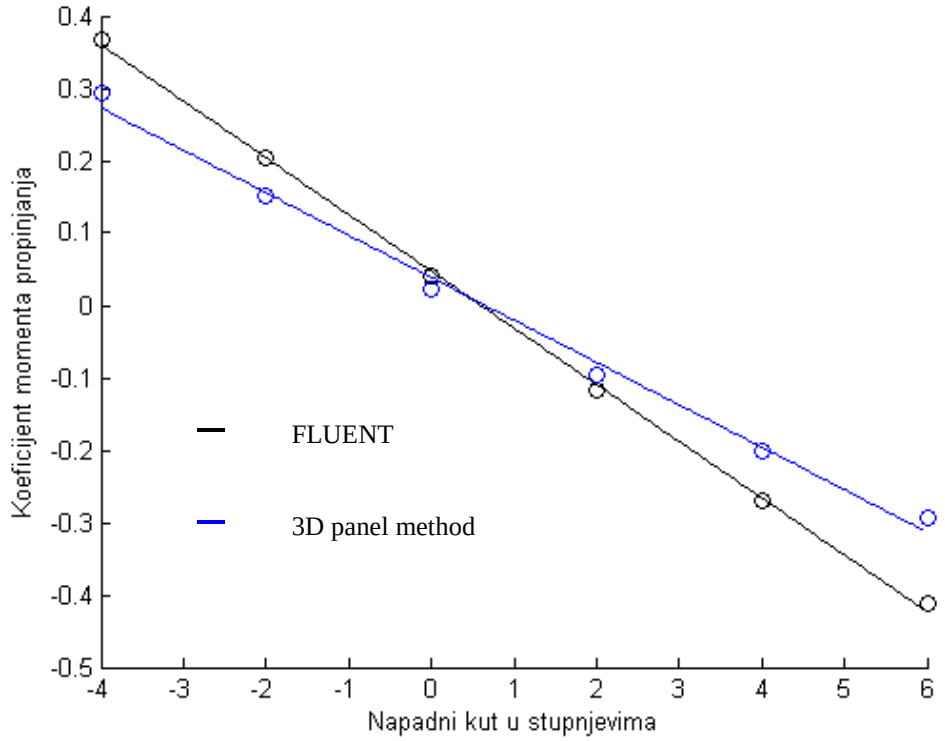

Diagram 4-17 Pitching moment coefficient vs. angle of attack

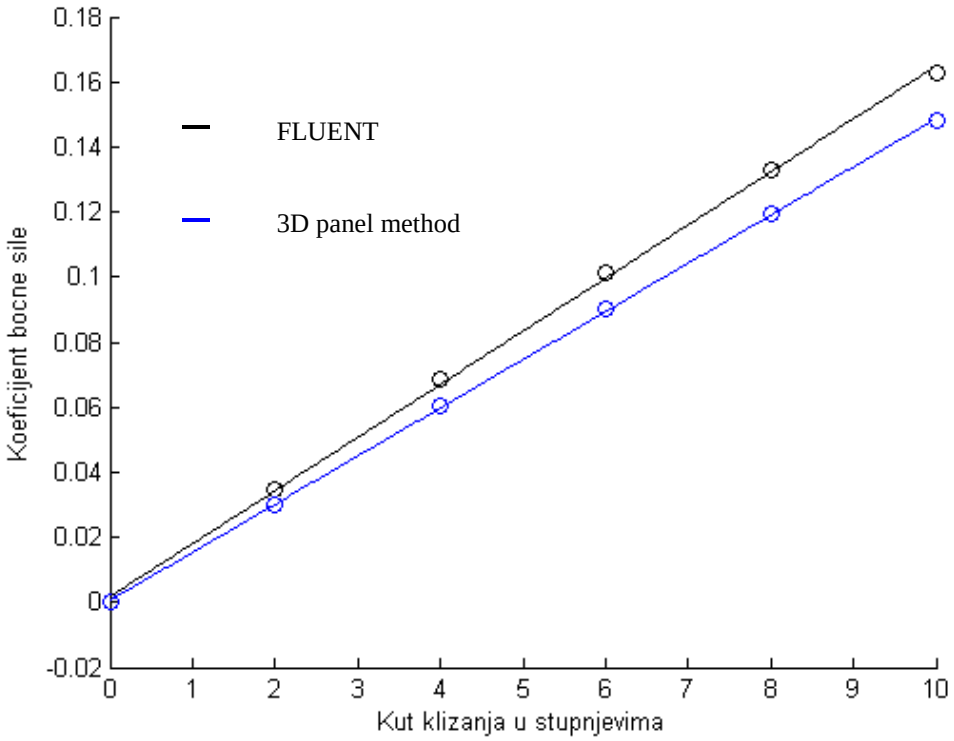

Diagram 4-18 Lateral force coefficient vs. sideslip angle

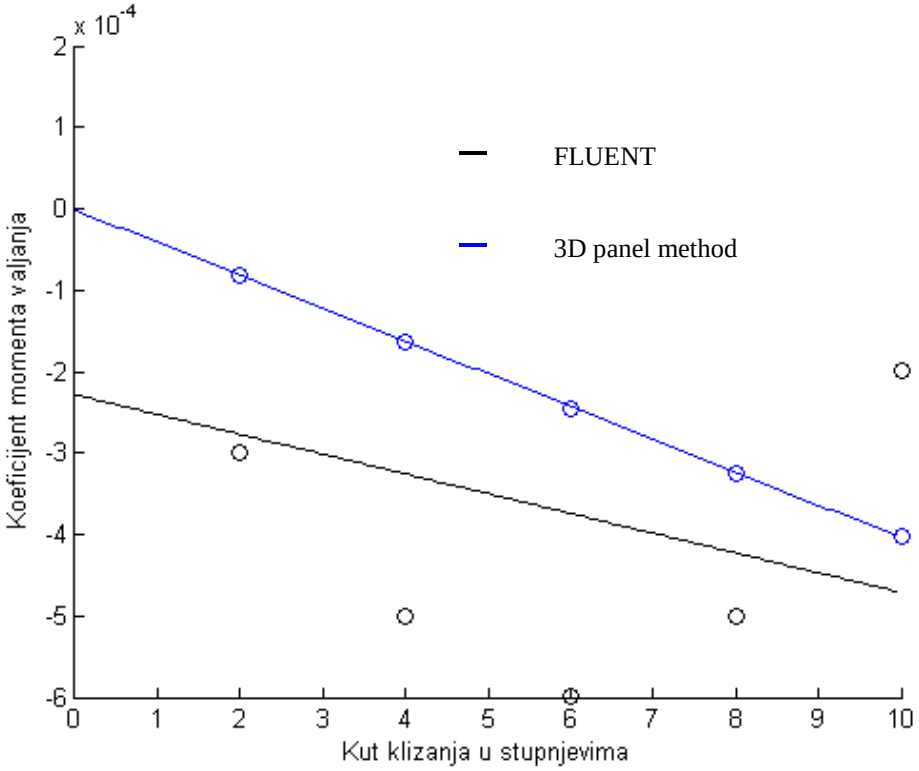

Diagram 4-19 Rolling moment coefficient vs. sideslip angle

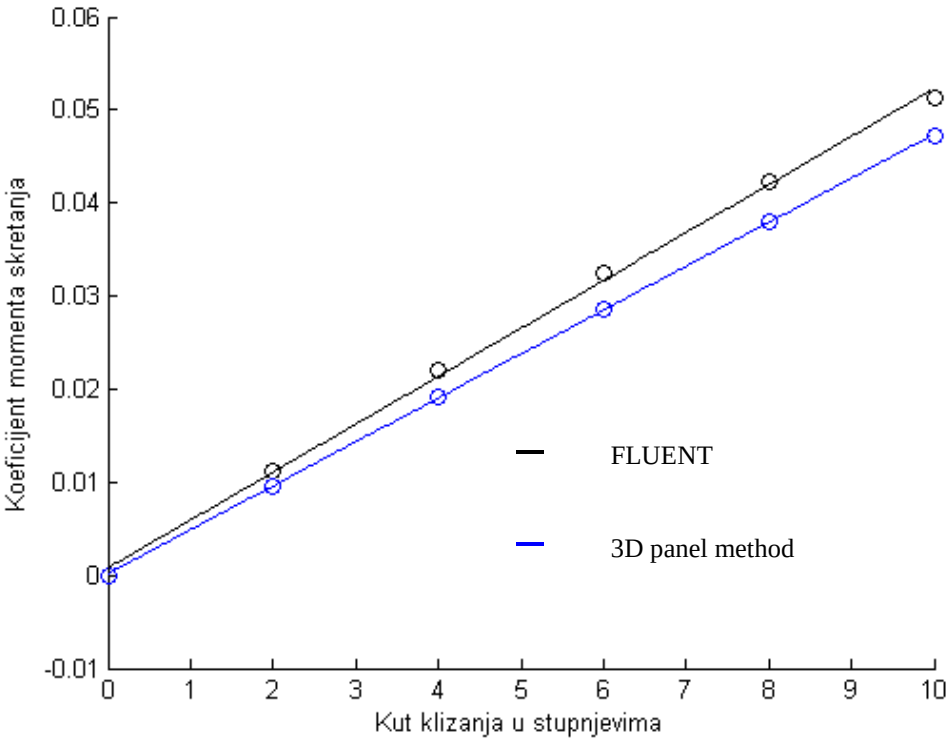

Diagram 4-20 Yaw moment coefficient vs. sideslip angle

From the previous diagrams a few extra conclusions can be made about behavior of coefficients. Minimum drag for potential flow in theory must be zero at angle at which the lift is also zero. It is evident from previous diagram (second diagram) that panel method gives minimal drag closer to zero, but negative, while FLUENT has some small positive minimal drag. Also, from previous diagram it might be said that similarity between rolling moment coefficients is bad, but since this is a very small size (also evident in Table 4-3) the difference can be ignored.

To gain better insight into results, all these values will be compared for each component of aircraft separately, first in table, after which discussion will be continued, and then through diagrams that will be left for the end of chapter because of their large number.

	horizontal stabilizer			vertical stabilizer			fuselage			wing			TOTAL		
	FLUENT	3D PM	diff [%]	FLUENT	3D PM	diff [%]	FLUENT	3D PM	diff [%]	FLUENT	3D PM	diff [%]	FLUENT	3D PM	diff [%]
C_{L0}	-0.0293	-0.0226	-23	-0.0001	0.0005	-633	0.0080	0.0012	-85	0.0939	0.0944	1	0.0725	0.0735	1
share [%]	-40	-31		0	1		11	2		130	128				
$C_{L\alpha}$	0.8632	1.0026	16	-0.0018	-0.0019	6	0.9356	0.2969	-68	4.1944	4.4683	7	5.9915	5.7658	-4
share [%]	14	17		0	0		16	5		70	77				
C_{D0}	0.0001	-0.0017	-2065	0.0015	0.0006	-61	0.0117	-0.0009	-107	0.0098	0.0000	-100	0.0231	-0.0020	\
share [%]	0	85		6	-29		51	43		42	-1				
e	4.3499	4.2020	-3	382.3710	-1225.40	-420	2.8640	1.2529	-56	1.6895	8.6854	414	0.8544	0.8737	2
C_{M0}	0.1218	0.0906	-26	0.0015	-0.0012	-180	-0.0096	0.0089	-193	-0.0667	-0.0600	-10	0.0471	0.0383	-19
share [%]	259	237		3	-3		-20	23		-142	-157				
$C_{M\alpha}$	-3.6995	-4.2865	16	-0.0035	-0.0036	3	0.7238	2.4890	244	-1.5113	-1.5559	3	-4.4899	-3.3574	-25
share [%]	82	128		0	0		-16	-74		34	46				

Table 4-4 Longitudinal analysis coefficients of aircraft components

	fuselage			vertical stabilizer			left horizontal stabilizer			right horizontal stabilizer		
	FLUENT	3D PM	diff [%]	FLUENT	3D PM	diff [%]	FLUENT	3D PM	diff [%]	FLUENT	3D PM	diff [%]
$C_{Y\beta}$	0.1698	0.1017	-40	0.7195	0.7014	-3	0.0035	0.0046	31	0.0169	0.0165	-2
share [%]	18	12		77	83		0	1		2	2	
$C_{l\beta}$	0.0165	0.0126	-24	-0.0634	-0.0630	-1	-0.0161	-0.0143	-11	-0.0160	-0.0139	-13
share [%]	-1179	-548		4529	2739		1150	622		1143	604	
$C_{n\beta}$	-0.0773	-0.0899	16	0.3529	0.3415	-3	0.0024	0.0029	21	0.0106	0.0108	2
share [%]	-26	-33		120	126		1	1		4	4	

	left wing			right wing			TOTAL		
	FLUENT	3D MP	diff [%]	FLUENT	3D MP	diff [%]	FLUENT	3D MP	diff [%]
$C_{Y\beta}$	0.0150	0.0139	-7	0.0108	0.011	2	0.9351	0.8487	-9
share [%]	2	2		1	1				
$C_{l\beta}$	0.0418	0.0412	-1	0.0354	0.0344	-3	-0.0014	-0.0023	64
share [%]	-2986	-1791		-2529	-1496				
$C_{n\beta}$	0.0025	0.0022	-12	0.0035	0.0029	-17	0.2952	0.2705	-8
share [%]	1	1		1	1				

Table 4-5 Lateral analysis coefficients of aircraft components

Consider wings. It can be seen that results of lift and pitching moment agree good while the results associated to drag are incomparable. If comparing results of left and right wings, especially in lateral analysis, good agreement is seen in all values including rolling moment coefficient gradient. Since on other components there is more or less good agreement, the cause of low values of rolling moment coefficient of the complete configuration for FLUENT (Figure 4-19) lies in adding up the amounts of all components whose result is near zero. Physically this can be explained by negative dihedral (adhedral) which annulled influence of vertical stabilizer making rolling moment coefficient gradient virtually non-existent. This phenomenon is also clearly evident from percentage of individual components (Table 4-5).

The horizontal stabilizer has clearly worse agreement than wings, which must be linked to "downwash" which deviates from real result of flat wake.

The vertical stabilizer shows good agreement in both, longitudinal and lateral analysis, except of course for drag.

Fuselage results are quite different, but this can be expected given the nature of method. While in FLUENT (inviscid flow, control volume method) each unsymmetrical body produces lift, and so does fuselage in this case, panel methods will produce lift only when Kutta condition is set (although panel method derived in this study gives a very small lift for fuselage while there is no Kutta condition and this can be attributed to numerical errors). Therefore, forces results on fuselage significantly differ since the only reasons for existence of forces in panel method is the influence of other bodies (mostly wings) and aforementioned numerical error. Unlike forces, moments in non-lifting bodies are present in panel method and somewhat higher due to fine asymmetrical pressure field over the body in potential flow, which can be seen in results.

When comparing results in diagrams, one must pay attention to size of coefficients of some components as they may be very small (such as lift coefficient for vertical stabilizer) and have no influence.

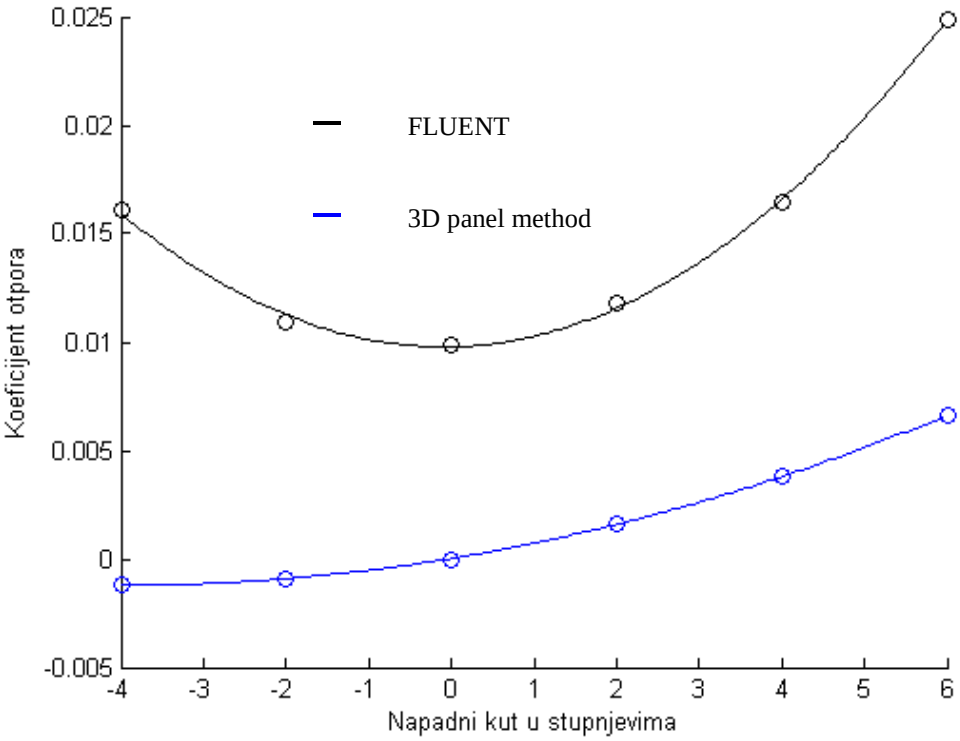

Diagram 4-21 Drag coefficient vs. angle of attack for wing

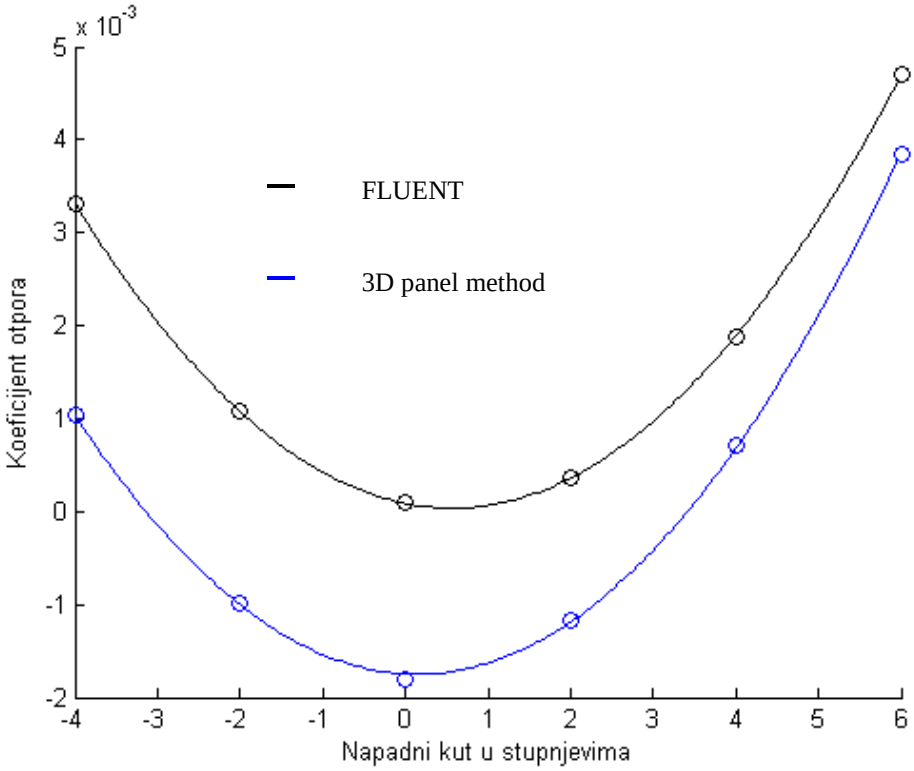

Diagram 4-22 Drag coefficient vs. angle of attack for horizontal stabilizer

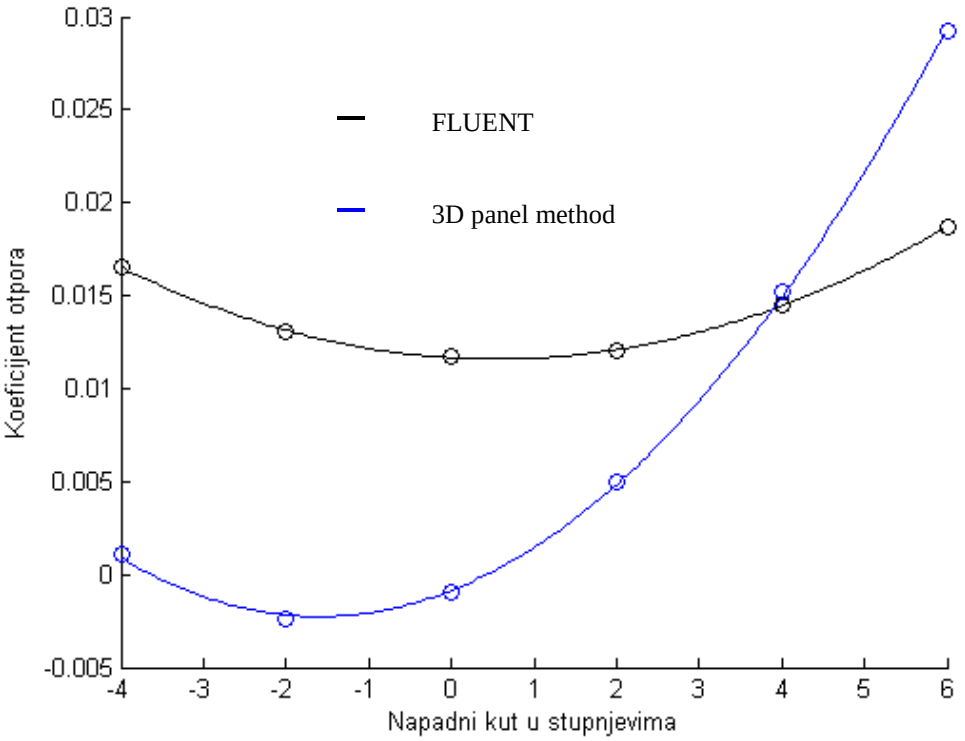

Diagram 4-23 Drag coefficient vs. angle of attack for fuselage

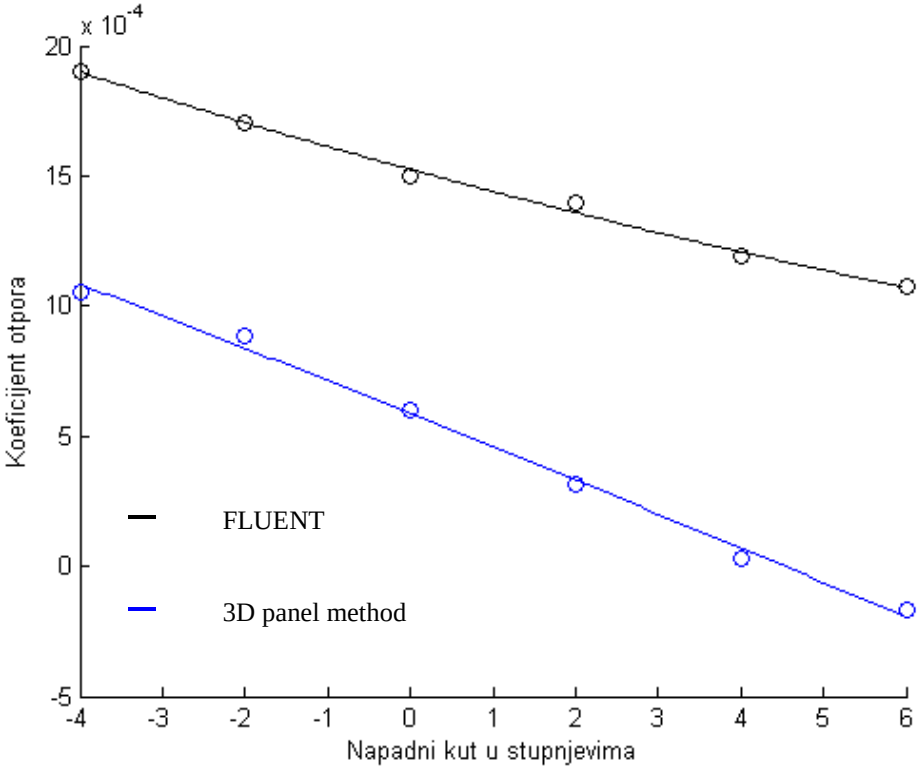

Diagram 4-24 Drag coefficient vs. angle of attack for vertical stabilizer

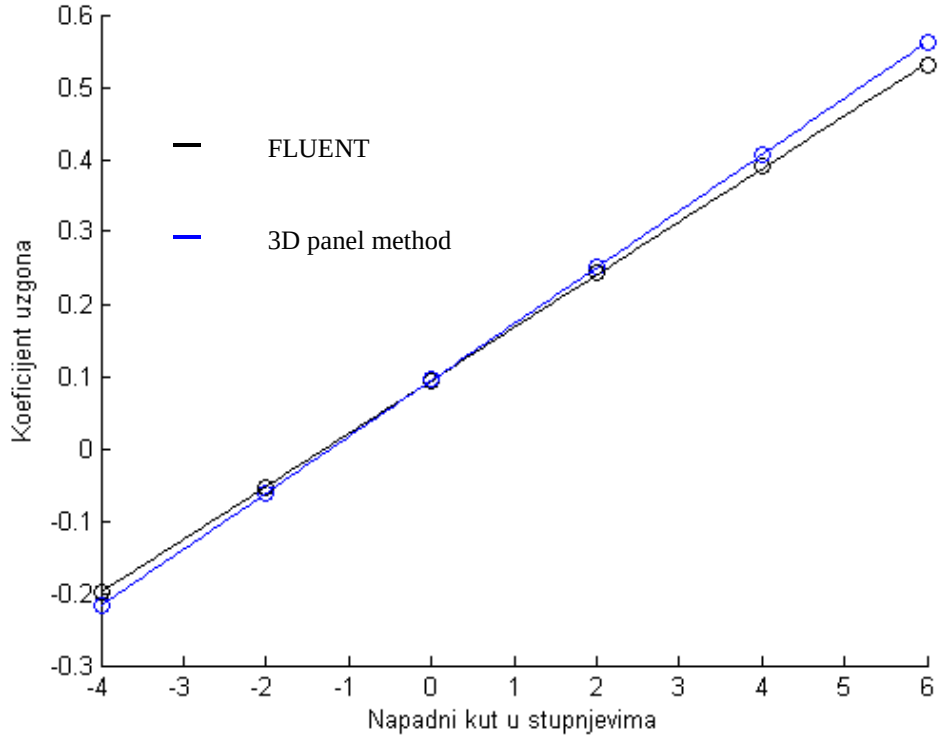

Diagram 4-25 Lift coefficient vs. attack of angle for wing

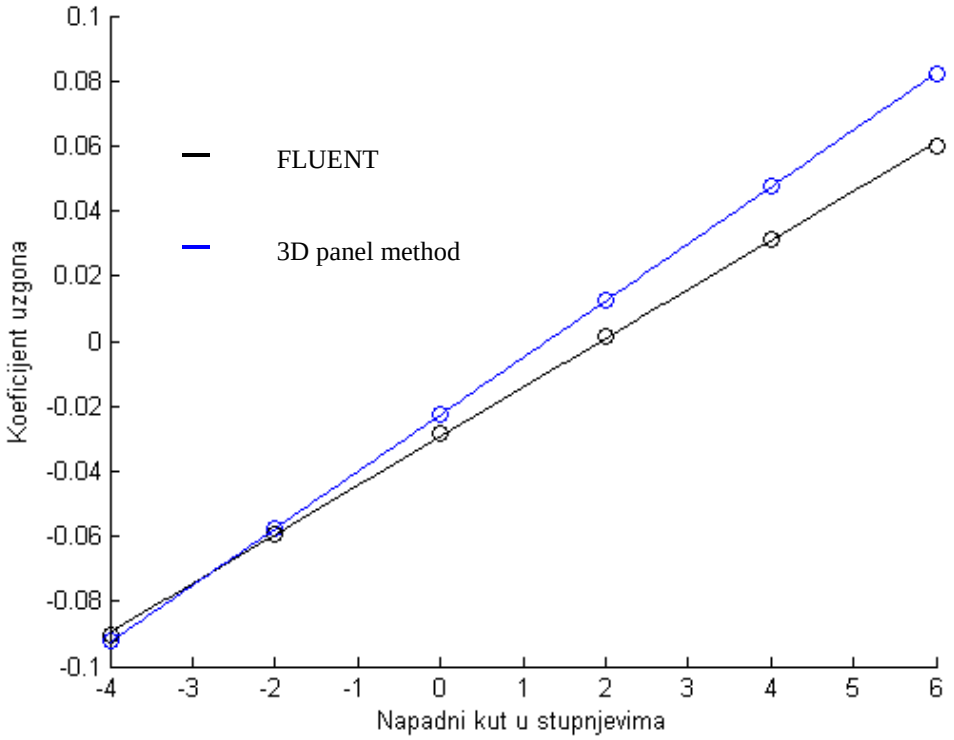

Diagram 4-26 Lift coefficient vs. angle of attack for horizontal stabilizer

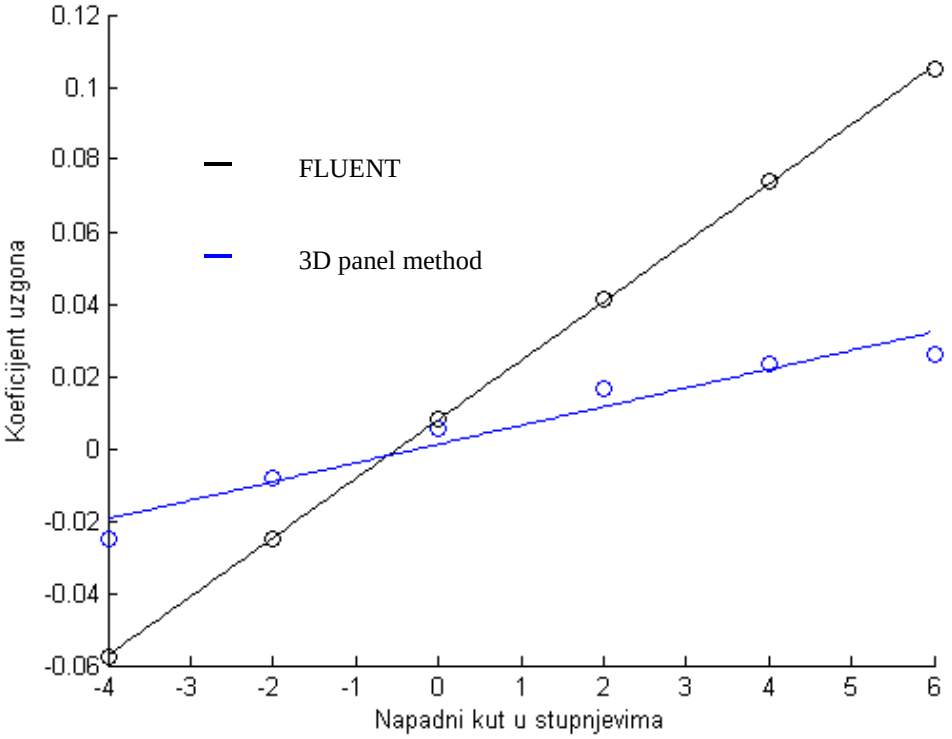

Diagram 4-27 Lift coefficient vs. angle of attack for fuselage

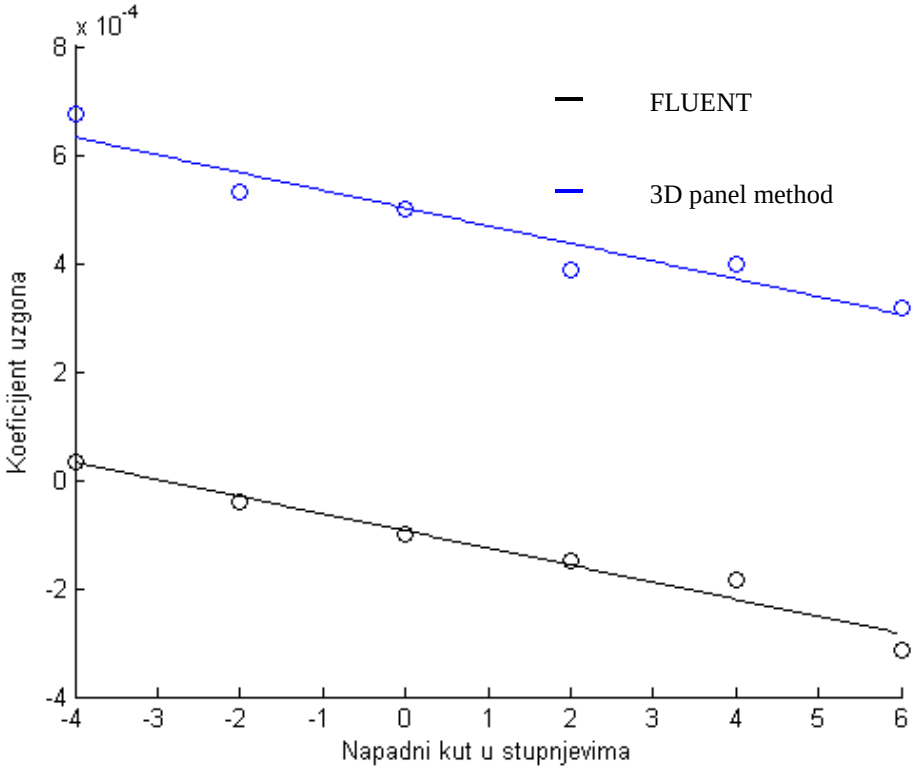

Diagram 4-28 Lift coefficient vs. angle of attack for vertical stabilizer

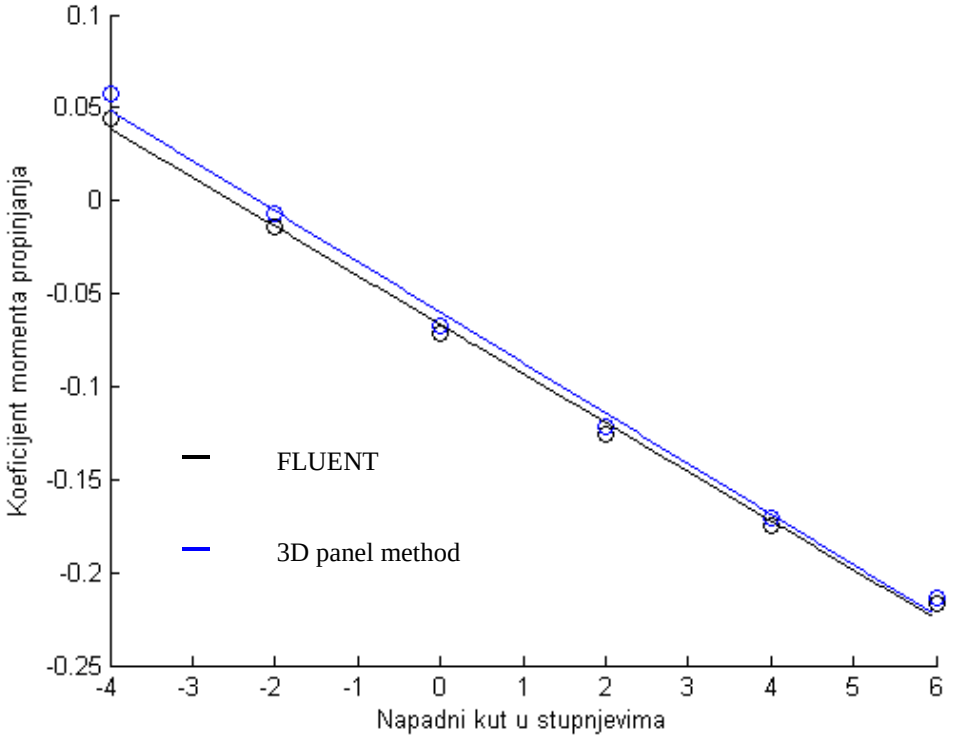

Diagram 4-29 Pitching moment coefficient vs. angle of attack for wing

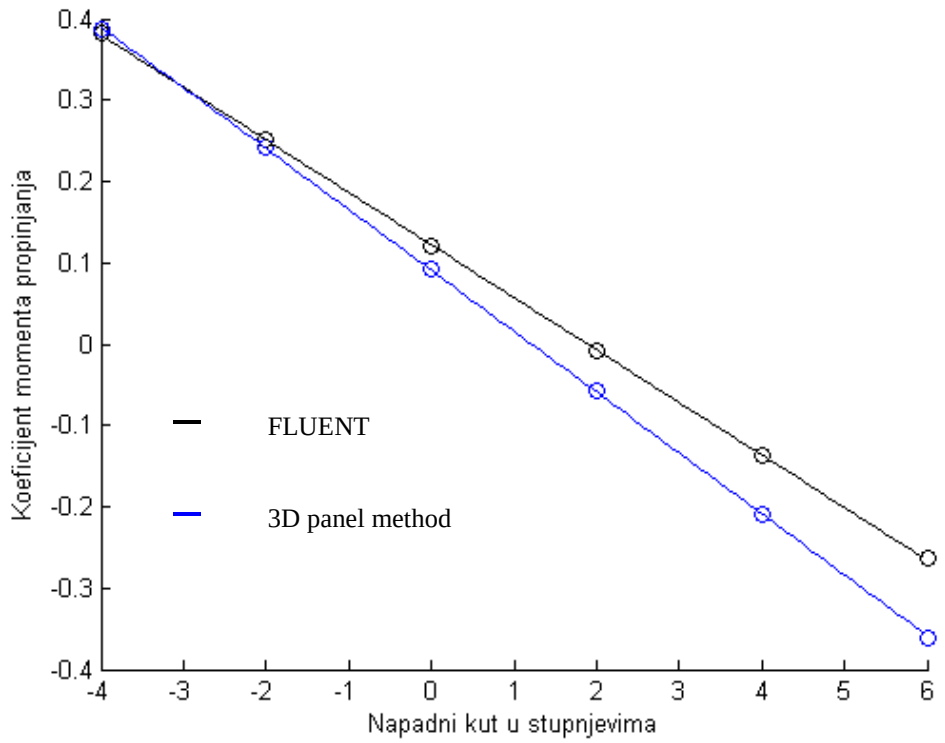

Diagram 4-30 Pitching moment coefficient vs. angle of attack for horizontal stabilizer

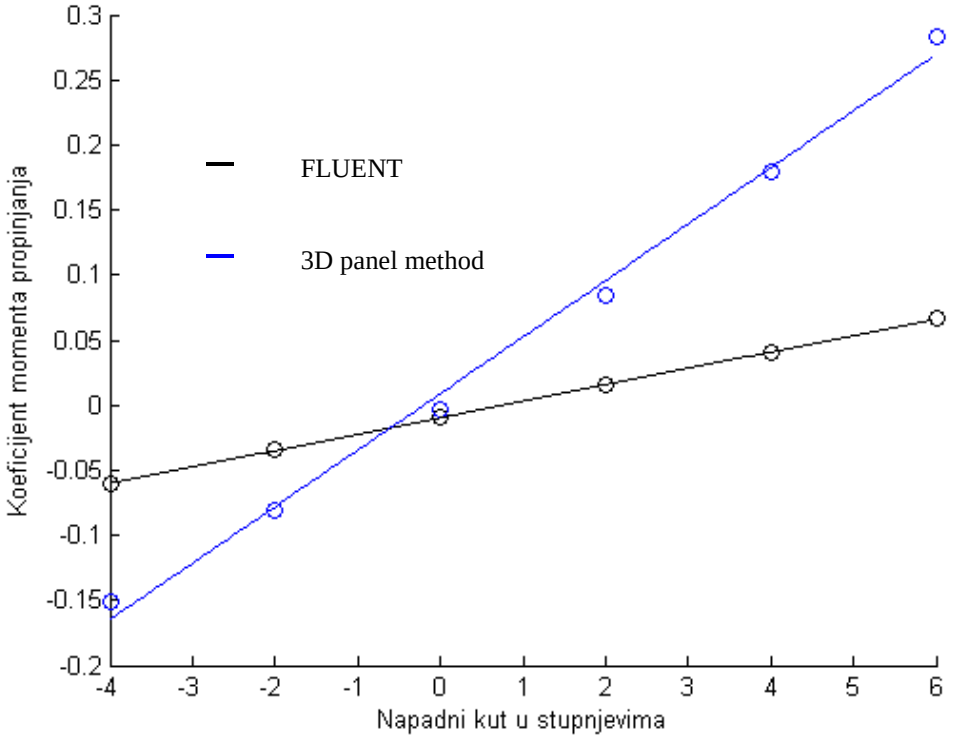

Diagram 4-31 Pitching moment coefficient vs. angle of attack for fuselage

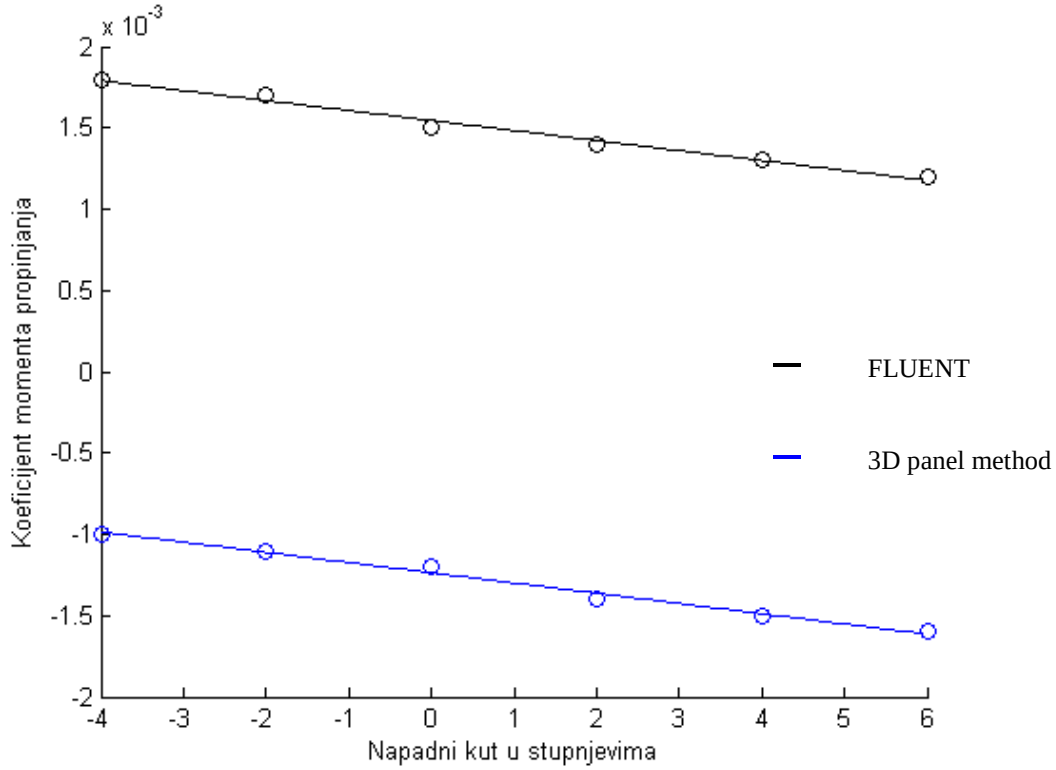

Diagram 4-32 Pitching moment coefficient vs. angle of attack for vertical stabilizer

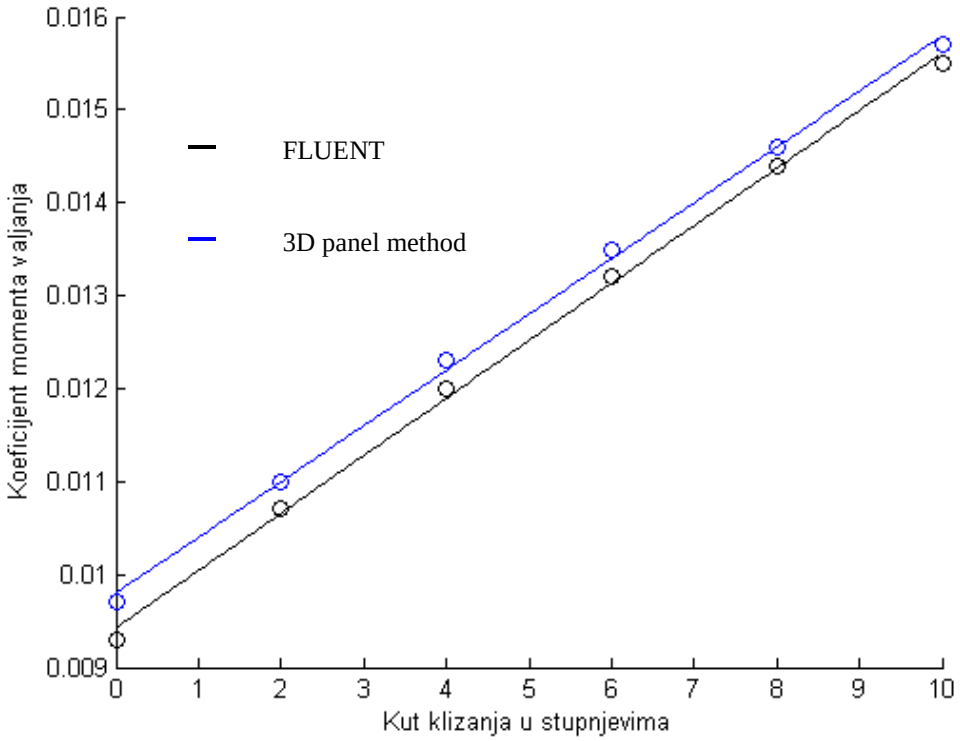

Diagram 4-33 Rolling moment coefficient vs. sideslip angle for right wing

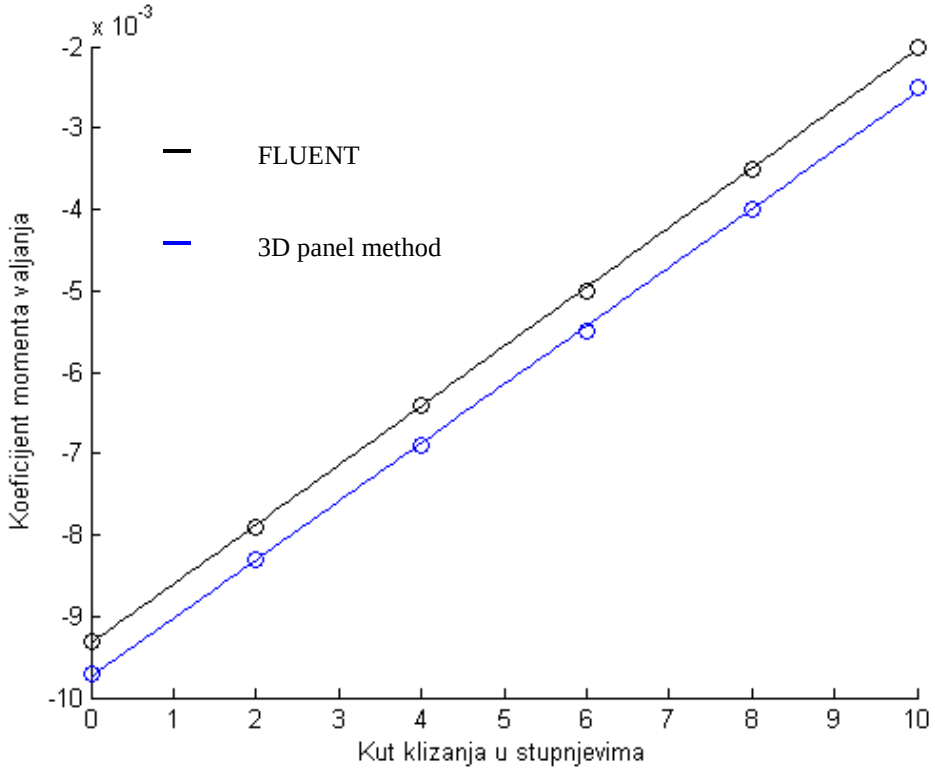

Diagram 4-34 Rolling moment coefficient vs. sideslip angle for left wing

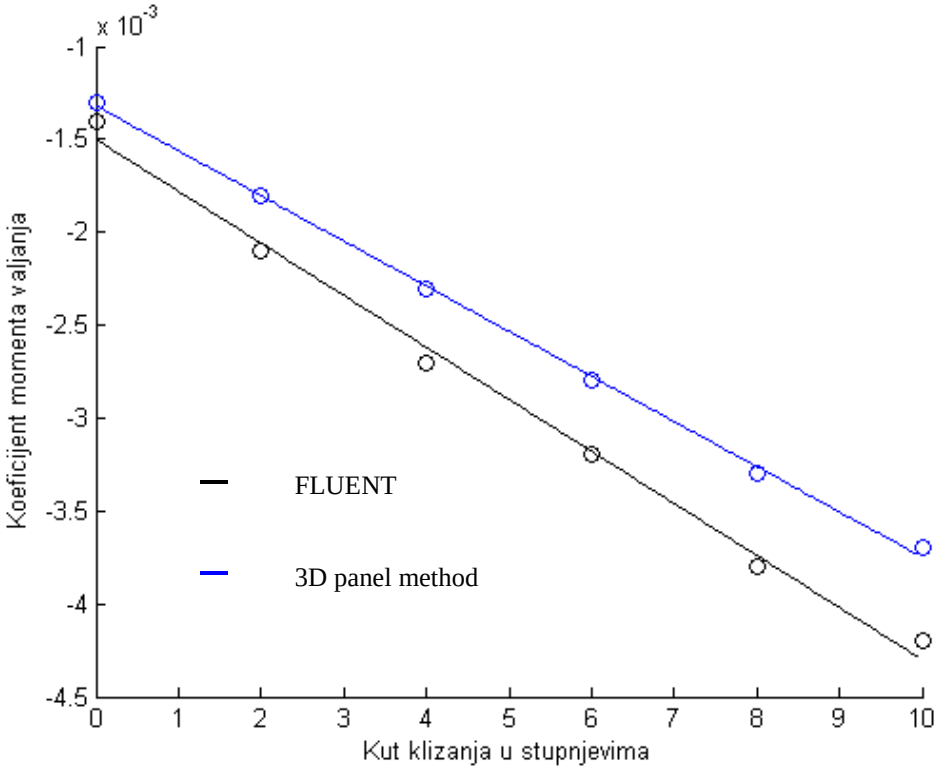

Diagram 4-35 Rolling moment coefficient vs. sideslip angle for right horizontal stabilizer

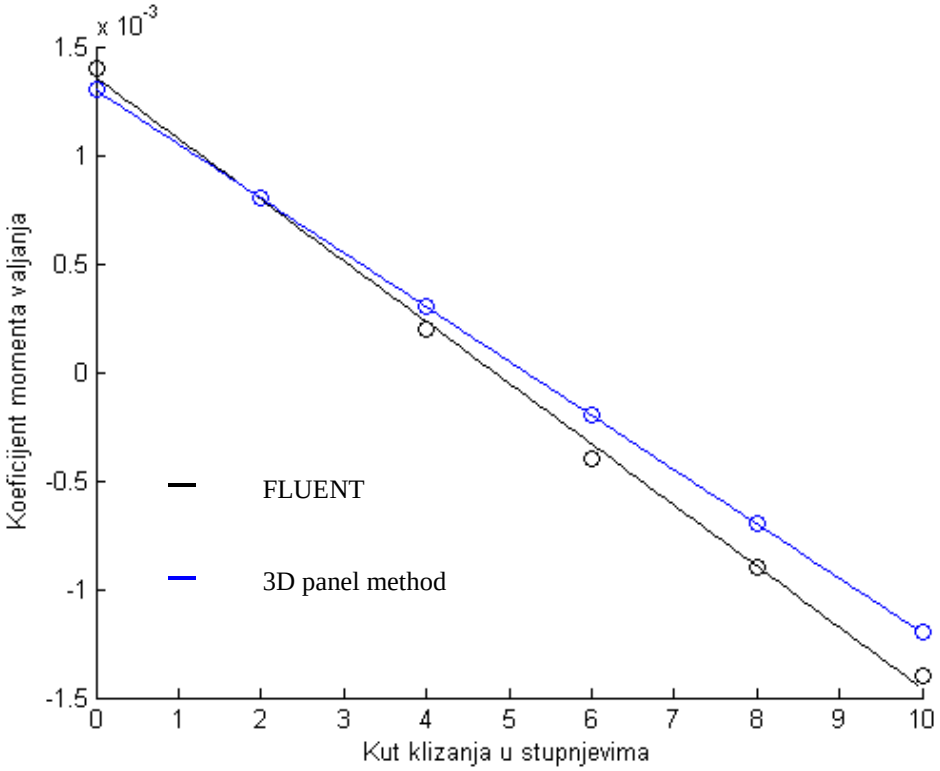

Diagram 4-36 Rolling moment coefficient vs. sideslip angle for left horizontal stabilizer

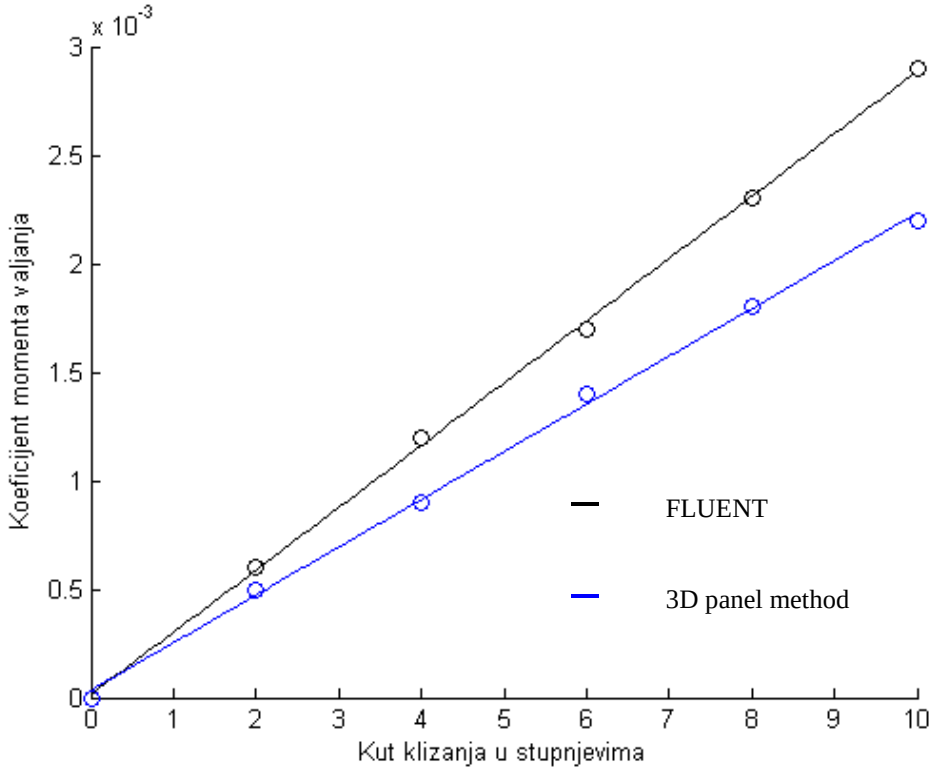

Diagram 4-37 Rolling moment coefficient vs. sideslip angle for fuselage

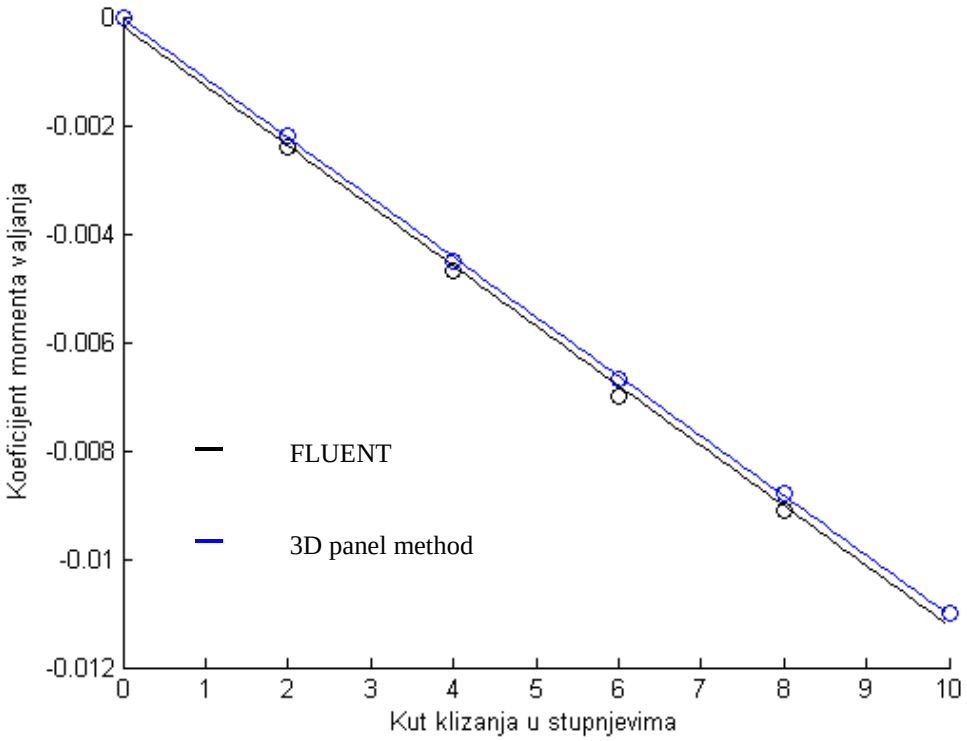

Diagram 4-38 Rolling moment coefficient vs. sideslip angle for vertical stabilizer

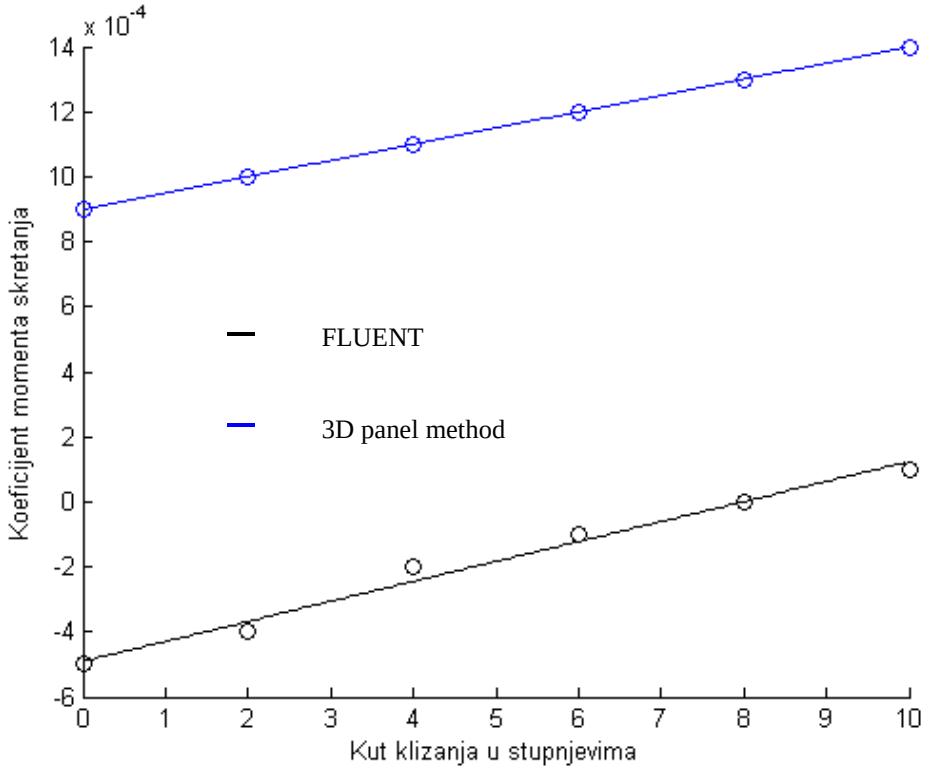

Diagram 4-39 Yaw moment coefficient vs. sideslip angle for right wing

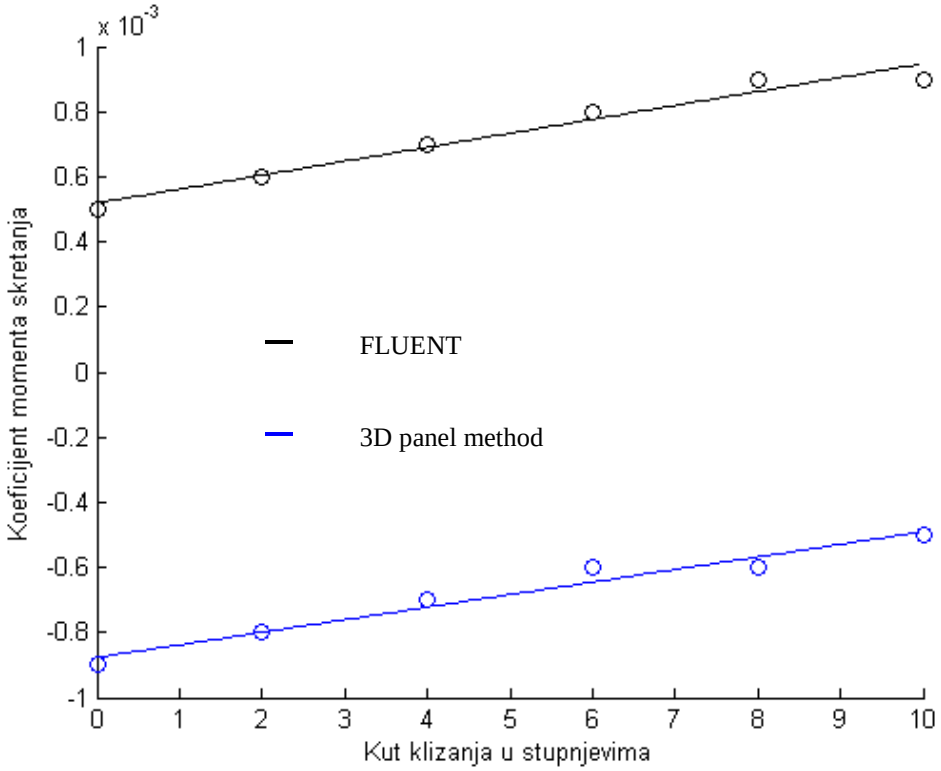

Diagram 4-40 Yaw moment coefficient vs. sideslip angle for left wing

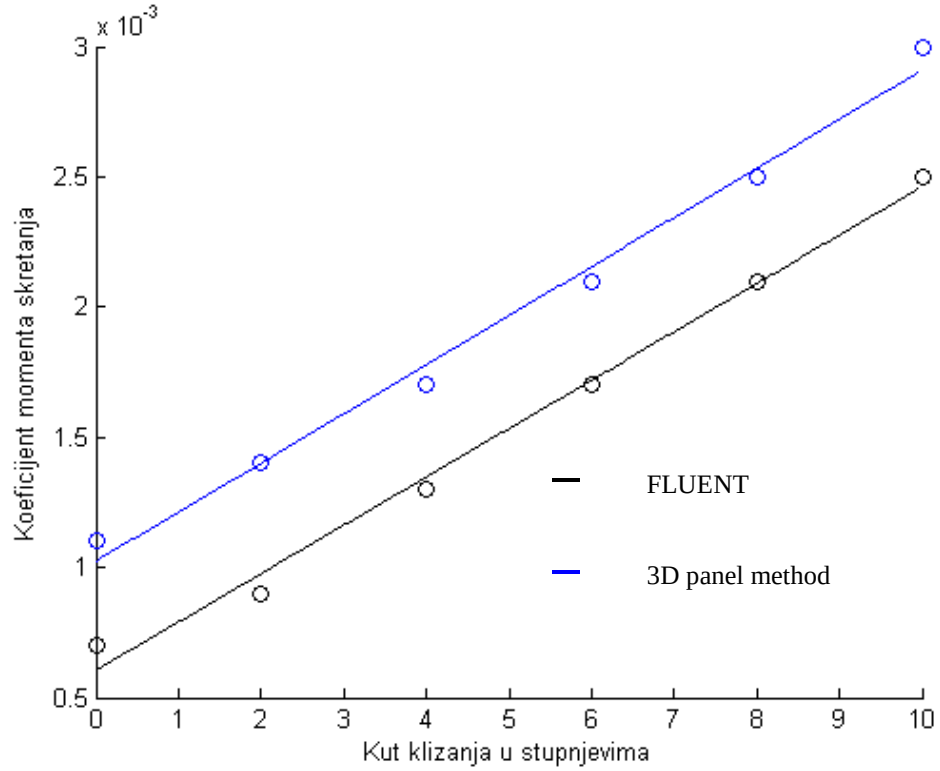

Diagram 4-41 Yaw moment coefficient vs. sideslip angle for right horizontal stabilizer

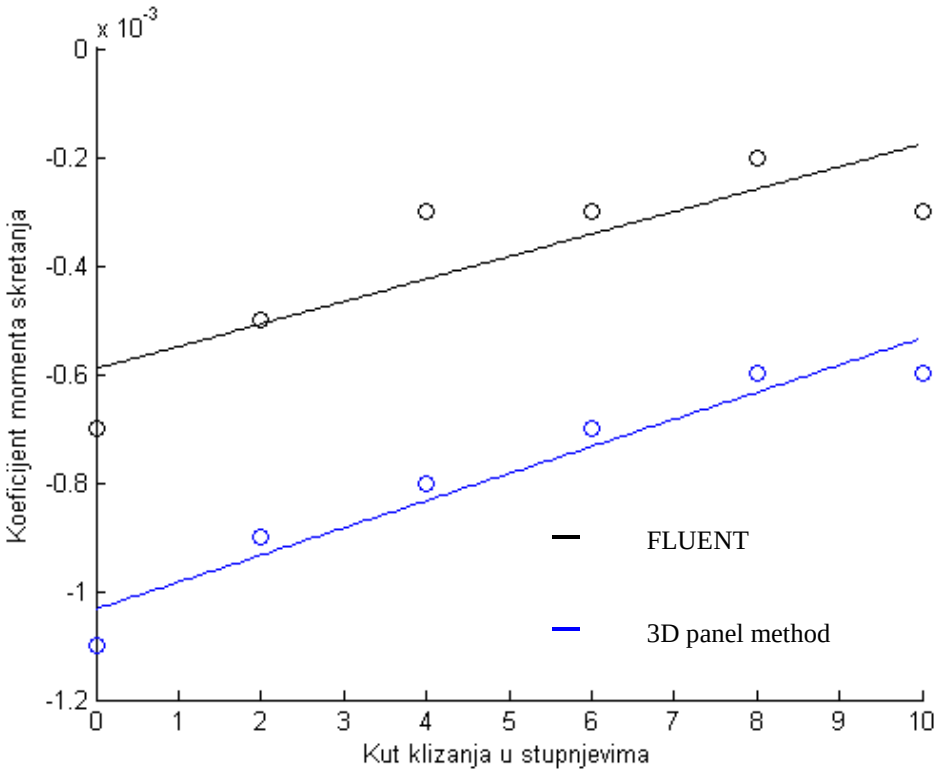

Diagram 4-42 Yaw moment coefficient vs. sideslip angle for left horizontal stabilizer

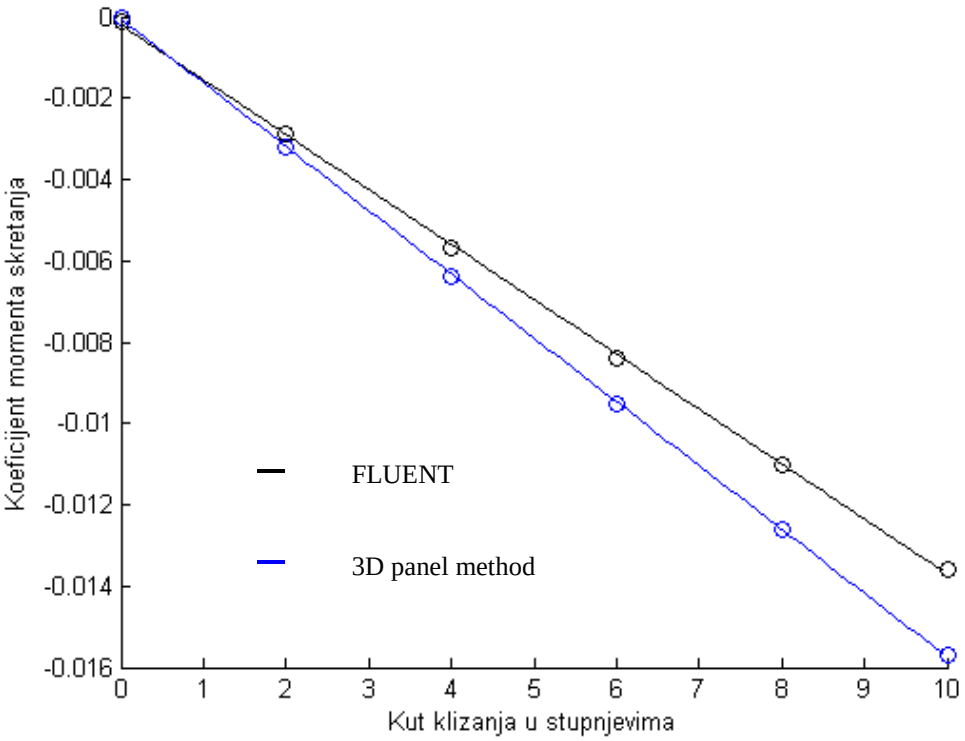

Diagram 4-43 Yaw moment coefficient vs. sideslip angle for fuselage

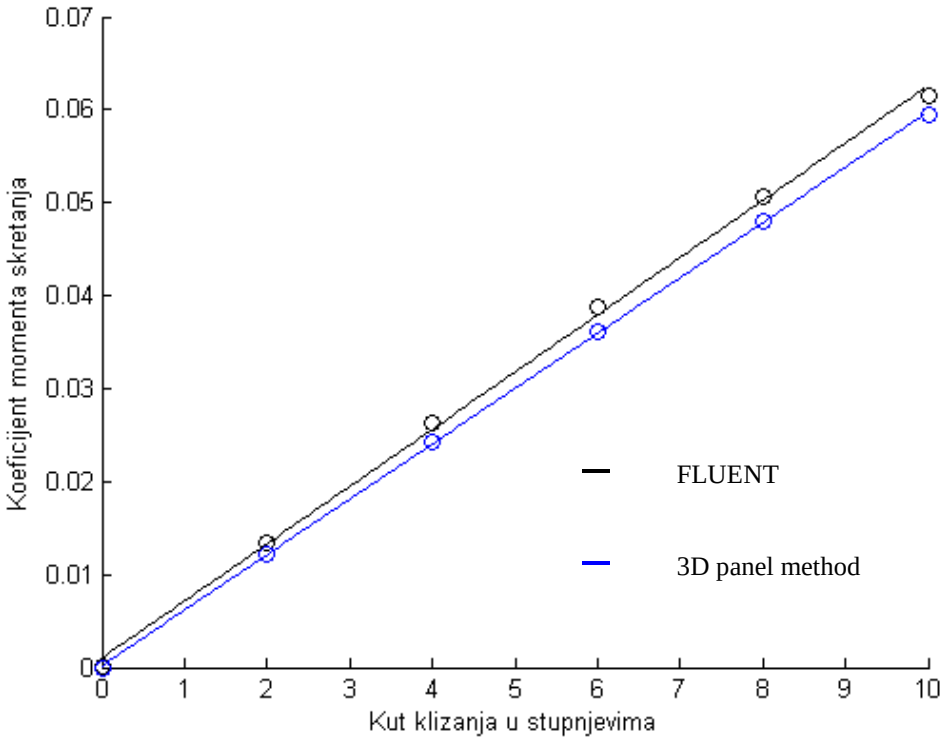

Diagram 4-44 Yaw moment coefficient vs. sideslip angle for vertical stabilizer

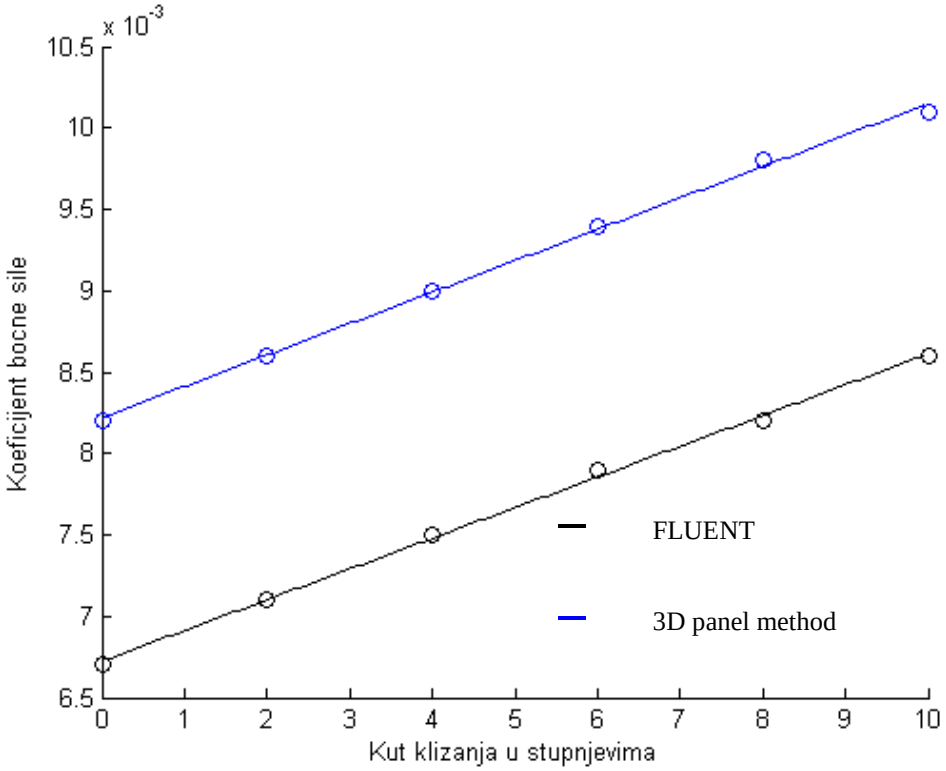

Diagram 4-45 Lateral force coefficient vs. sideslip angle for right wing

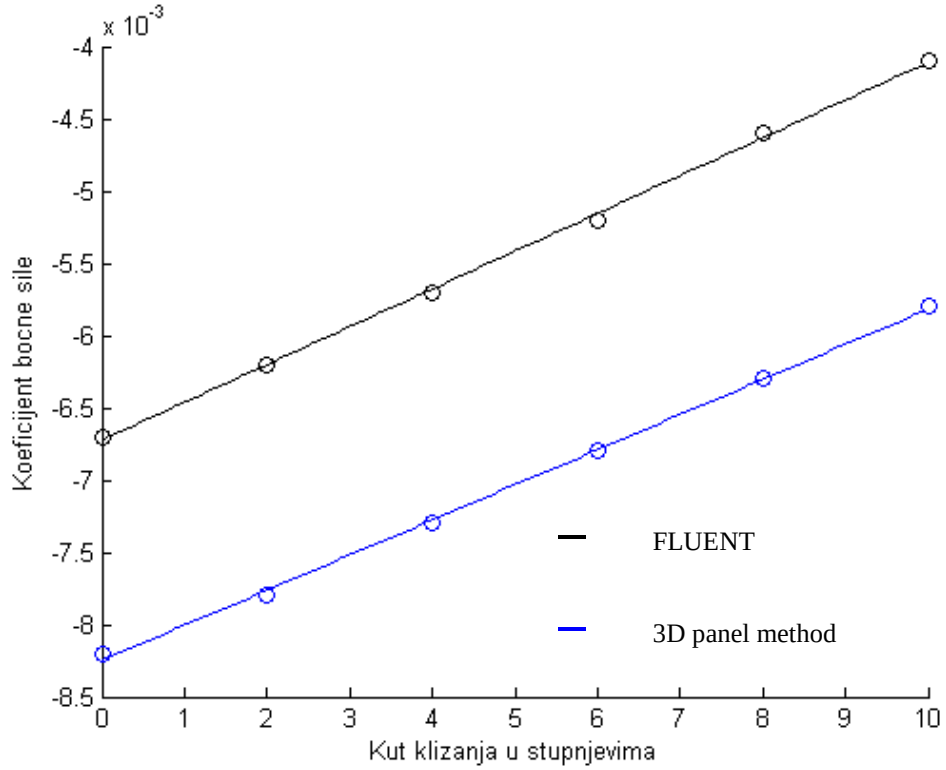

Diagram 4-46 Lateral force coefficient vs. sideslip angle for left wing

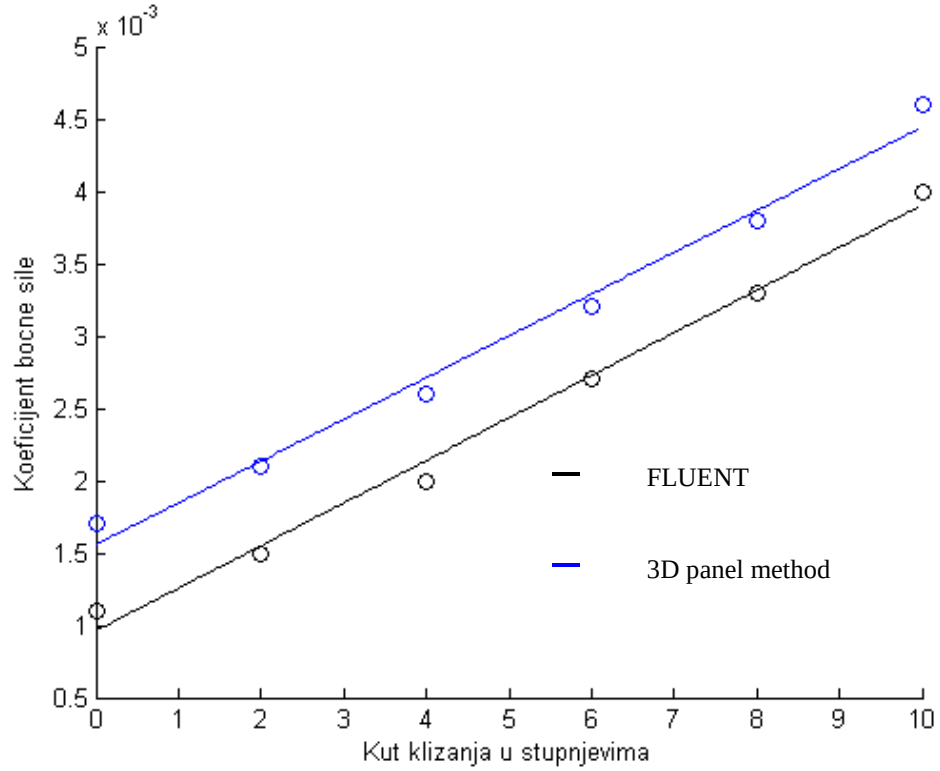

Diagram 4-47 Lateral force coefficient vs. sideslip angle for right horizontal stabilizer

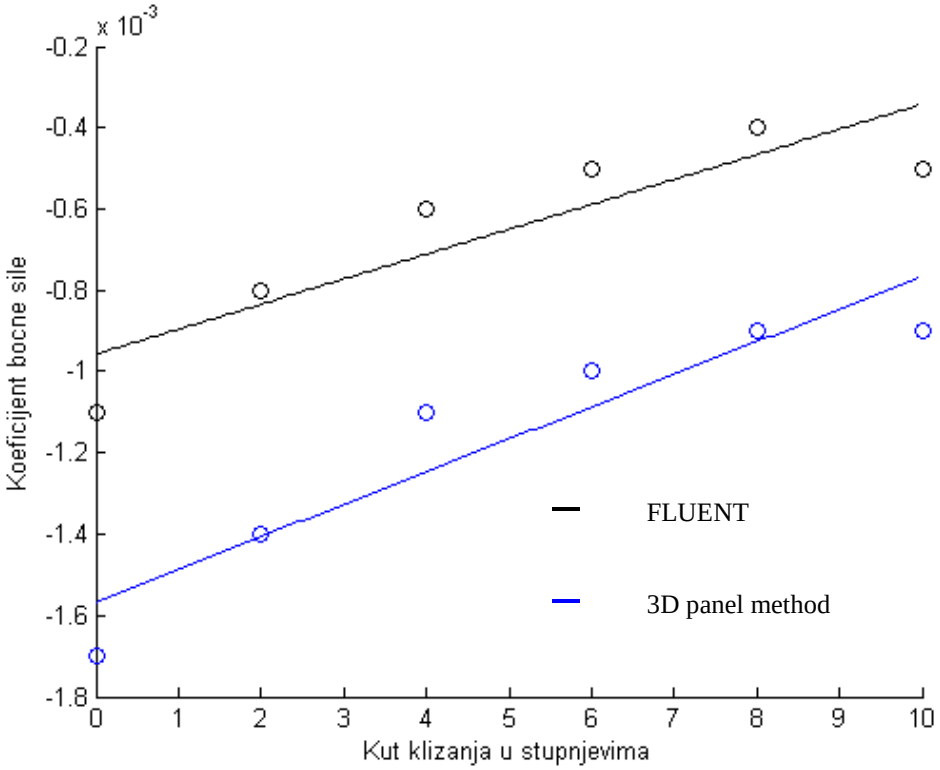

Diagram 4-48 Lateral force coefficient vs. sideslip angle for left horizontal stabilizer

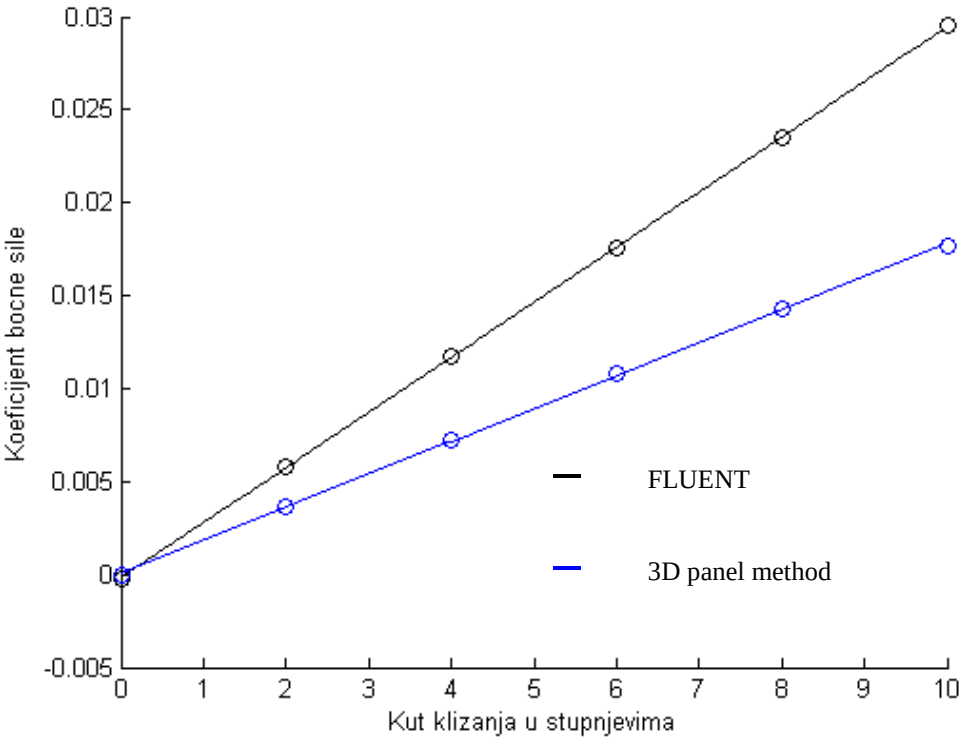

Diagram 4-49 Lateral force coefficient vs. sideslip angle for fuselage

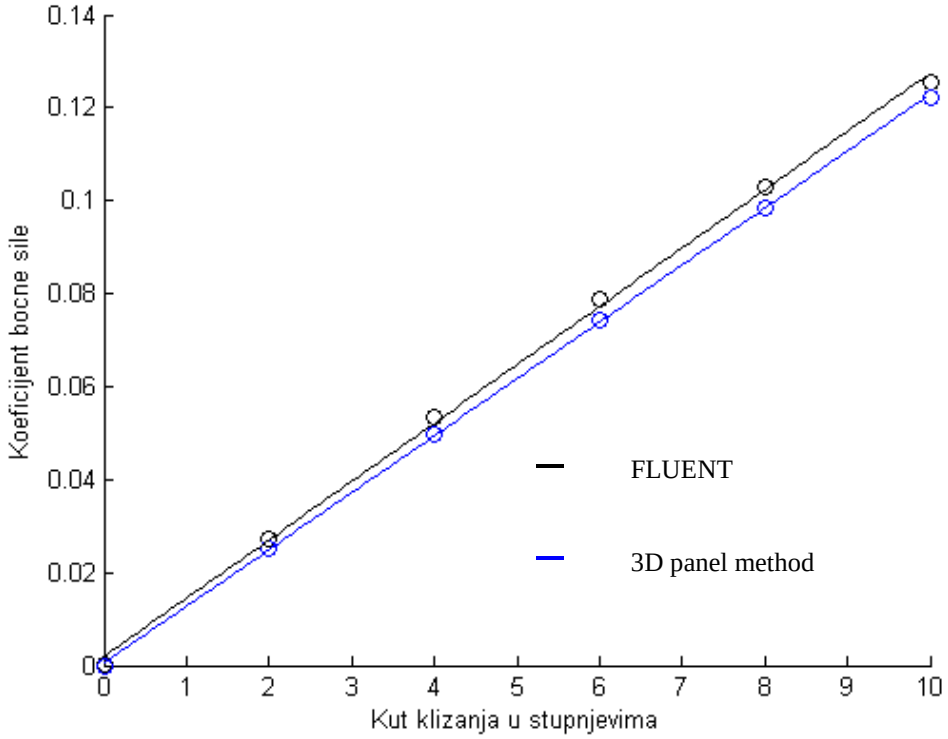

Diagram 4-50 Lateral force coefficient vs. sideslip angle for vertical stabilizer

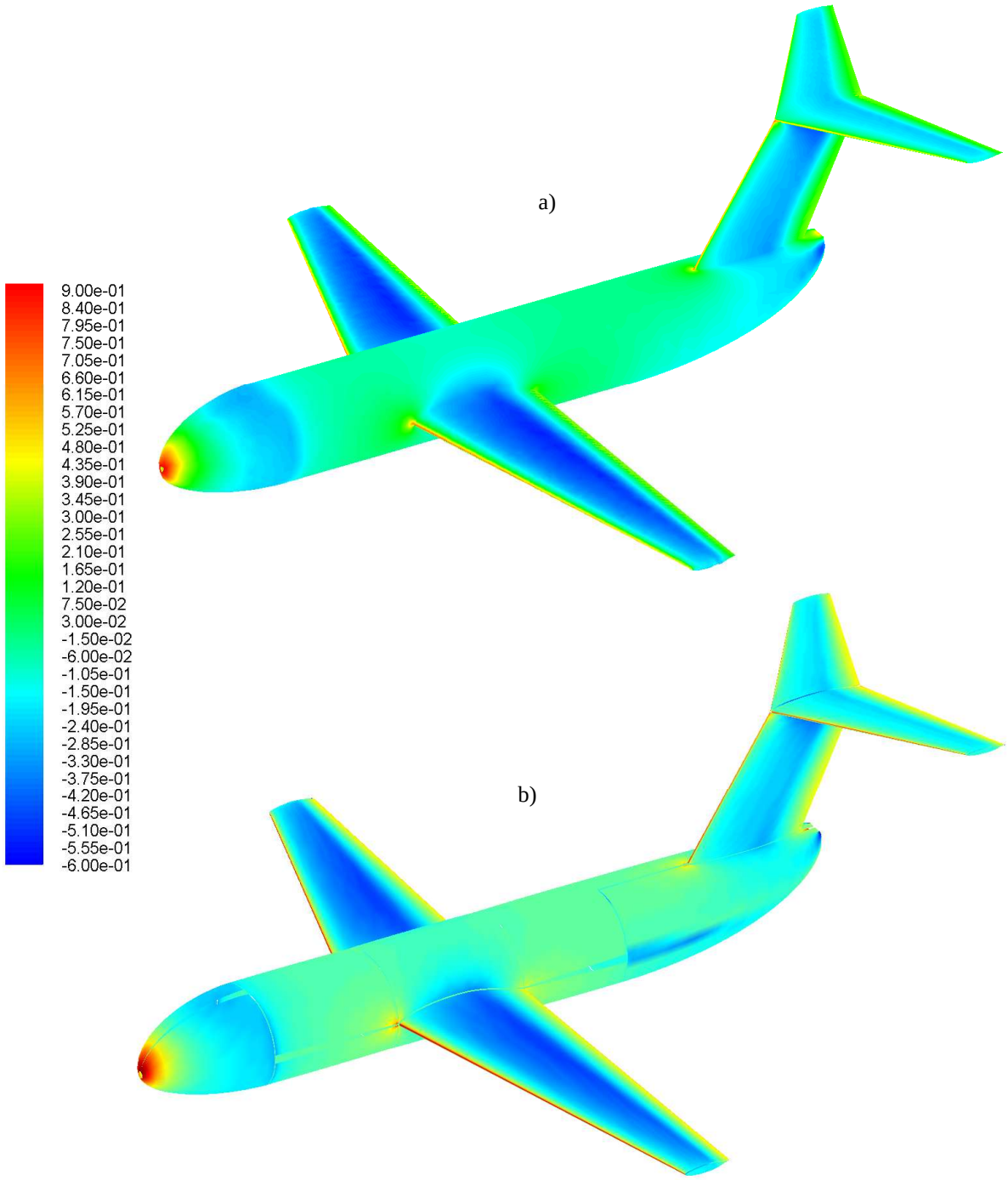

Figure 4-8 Pressure coefficient distribution for a) FLUENT b) 3D Panel Method

CONCLUSION

This paper presents the possibility of calculating aerodynamic configuration of aircraft using 3D panel method. The results are compared with results from a commercial package FLUENT and extensively described by diagrams of aerodynamic coefficients.

It can be concluded that, if we exclude results associated to drag, results of the 3D panel methods are in good match with results from FLUENT. Very good match related to lift is obtained for the wings, or more generally, for all bodies on which Kutta condition can be set. Based on results, conclusions can be made that for all coefficients, except the drag and pitching moment coefficients, difference falls below 10%, drag coefficient is incomparable, and results for pitching moment differ about 20% for complete configuration.

Observed deficiencies could be eliminated by:

- Adjusting the wake. Two methods are possible: The first method iteratively moves wake points using induced velocities in them, while second transient and iterative method starts with a still state and then with every subsequent iteration new wake points are inserted

Extension of program features could be achieved by:

- Using second method of wake adjusting, since this method can calculate unsteady aerodynamic coefficients
- Adding boundary layer calculation, where pressure and velocity fields are used as input in calculation of viscous friction near wall from which a very significant component of drag is found – friction drag.

Using these two corrections, a powerful tool for complete definition of aerodynamic behavior of aircraft in linear regime (angle of attack of about -6 to +6 and sideslip angle from -10 to +10 degrees) could be made for incompressible flow, therefore to ~0.3Ma. In this case method would be more reliable as body would be more aerodynamically shaped, or with less blunt bodies such as fuselage where Kutta condition cannot be set or its setting would not result in correct flow.

Literature

[1] Katz J, Plotkin A, Low Speed Aerodynamics - Second edition, Cambridge University Press, New York, 2001.

[2] Kesić P, Osnove aerodinamike, Fakultet strojarstva i brodogradnje, Zagreb, 2003.

[3] Janković S, Mehanika leta zrakoplova, Fakultet strojarstva i brodogradnje, Zagreb, 2002.

[4] Abbott I H, Doenhoff A E, Theory of wing sections, Dover Publications Inc, New York, 1959.

[5] Aerodinamika I, Web materials, Faculty of Mechanical Engineering and Naval Architecture, Zagreb, http://www.fsb.hr/hydro/web_sites/Popis%20predmeta/Aerodinaika1.htm